Energy Conversion and Management: X 28 (2025) 101225

Contents lists available at ScienceDirect

Energy Conversion and Management: X

journal homepage: www.sciencedirect.com/journal/energy-conversion-and-management-x

Adaptive optimal disturbance rejection for wave energy converters

Kumars Mahmoodi [a,*], Abolhassan Razminia [b], Jari Böling [c]

[a] Process Control Laboratory, Faculty of Natural Sciences and Engineering, Åbo Akademi University, Turku, Finland
[b] Department of Electrical Engineering, Faculty of Intelligent Systems Engineering and Data Science, Persian Gulf University, Bushehr, Iran
[c] Automation, Mechanical and Materials Engineering, University of Turku, Finland

ARTICLE INFO

Keywords:
Adaptive control
Optimal control
Disturbance rejection
Wave energy converter
Nonlinear Autoregressive Neural Network

ABSTRACT

This research aims to mitigate disturbances affecting Wave Energy Converters (WECs) using an adaptive optimal disturbance rejection framework by dynamically adjusting control actions based on forecasted wave conditions. A Nonlinear Autoregressive (NAR) Neural Network is utilized for forecasting wave elevations and generating optimal reference velocities for the considered case study single-body heaving point absorber. The wave excitation force is considered as the external disturbance source affecting the WEC. Frequency and time domain response analysis are conducted to understand system behavior, followed by considering the real wave climate of two different selected locations around Finland, crucial for performance evaluation. The efficacy of the proposed approach is evaluated through a comprehensive results analysis. This includes evaluating its effectiveness on the selected sea states and its adaptability concerning variations in WEC dynamics. In all the investigated scenarios, the proposed control strategy can track the displacement and velocity reference signals with high accuracy in the presence of disturbance with proper initializing of the weight matrices, highlighting the potential of the proposed methodology in improving the efficiency and reliability of WECs under varying wave conditions.

1. Introduction

The harnessing of renewable energy sources has become an imperative in the quest for a sustainable and environmentally responsible future. Among these sources, ocean waves stand out as a largely untapped reservoir of energy [1–3]. WECs play a pivotal role in extracting this energy that offers the promise of clean and consistent power generation [4,5]. However, the optimal performance of WECs is challenged by the ever-changing nature of oceanic disturbances [6], which can significantly affect their efficiency and reliability.

Wave disturbances can significantly impact the operation of WECs, leading to suboptimal energy conversion and potentially damaging mechanical stress. Ocean waves exhibit inherent variability in terms of amplitude, frequency, and direction [7], which can create disturbances in the motion of WECs. Variations in wave height, period, and shape can lead to fluctuations in the input energy, affecting the operation of WEC devices. On the other hand, environmental factors such as wind speed, current velocity, and water depth can influence wave characteristics and introduce disturbances in WEC operation [8,9]. Interactions between incoming waves, such as wave reflection, refraction, and diffraction, can cause interference patterns that affect the motion of WEC devices. Wave interference can result in complex wave fields, leading to non-uniform loading and disturbances in WEC performance [10].

Extreme waves can cause intense wave-structure interactions, characterized by wave slamming, wave overtopping, and wave-induced motions of WEC devices. These interactions generate transient disturbances in the form of impact forces, hydrodynamic pressures, and structural vibrations, which can impact the operational efficiency and structural integrity of WEC systems. These nonlinear effects can introduce additional complexities in the interactions between waves and WEC devices, resulting in irregular and unpredictable disturbances in device motion [11]. Moreover, external factors such as marine debris, marine life interactions, or human activities in the vicinity of WEC installations can introduce disturbances that interfere with device operation [12]. These external interferences may cause mechanical damage, fouling, or operational disruptions, impacting the reliability of WEC systems. Addressing these factors and mitigating disturbances is crucial for optimizing the performance and reliability of WECs. Advanced control strategies [13–15], predictive modeling techniques [6,16], and robust design considerations are essential for minimizing the impact of disturbances and maximizing the energy conversion efficiency of WECs in real-world operating conditions.

* Corresponding author.
E-mail addresses: kumars.mahmoodi@abo.fi (K. Mahmoodi), razminia@pgu.ac.ir (A. Razminia), jari.boling@utu.fi (J. Böling).

https://doi.org/10.1016/j.ecmx.2025.101225
Received 13 June 2025; Received in revised form 9 August 2025; Accepted 24 August 2025
Available online 31 August 2025

Advanced control strategies are essential to optimize the performance of WEC systems in varying sea conditions. Control strategies enable WECs to track incoming wave conditions in real-time and adapt their operation accordingly [17]. By adjusting parameters such as the geometry, orientation, or damping of the WEC, it can be tuned to efficiently capture the energy from different wave patterns [15,18]. Many WEC designs rely on resonance phenomena to enhance energy capture. Control strategies are employed to maintain the device's resonance with the incident waves by adjusting the device's natural frequency or damping characteristics. Control algorithms can optimize the PTO system [19] to extract the maximum amount of energy from the waves. This involves continuously adjusting the loading on the WEC's PTO mechanism to match the varying wave characteristics and maintain resonance or near-resonance conditions. Control strategies can incorporate wave forecasting data [20] to predict future wave conditions. By anticipating incoming waves, the WEC can adjust its settings preemptively to optimize energy capture and minimize the impact of irregular or extreme waves. However, control theories have some weaknesses. Control systems used to regulate the operation of WEC devices may have limitations in terms of response time, accuracy, and robustness. Inaccuracies in control algorithms or delays in feedback signals can result in disturbances that affect the ability of WECs to efficiently capture wave energy.

Recent literature has proposed a broad range of data-driven control strategies in wave energy applications, including model-free reinforcement learning [21–23], neural-network-based predictive control [24–27], and hybrid data-physics [28] models. For a more structured overview, the work [29] provides a comprehensive classification of such methods, categorizing them based on data dependency, adaptability, and feedback structure. Adaptive control techniques [30–32], including machine learning algorithms, can continuously learn from operating data to improve WEC performance over time [33]. By adapting control strategies based on real-time feedback and historical performance data, these approaches enable WECs to optimize energy capture in varying sea conditions and adapt to changing environmental factors [34,35]. Adaptive control techniques facilitate the identification of WEC parameters, such as hydrodynamic coefficients, natural frequencies, and damping ratios, which are essential for accurate modeling and control. By continuously updating these parameters based on operating data, adaptive control ensures that the control system remains effective under varying environmental conditions and system configurations.

In addition to forecasting-based and data-driven control approaches, disturbance observer techniques have been applied to enhance robustness in dynamic systems subject to external disturbances. Such methods aim to estimate and compensate for unmeasured disturbance inputs in real time, improving control performance under uncertainty [36,37]. Incorporating such observer-based strategies into WEC control frameworks can complement forecasting and estimation methods, leading to improved performance in realistic, disturbance-rich ocean environments [38–40].

This research explores the domain of adaptive optimal disturbance rejection for WECs, a crucial aspect in ensuring their effectiveness and resilience against dynamic ocean conditions. Traditional control strategies often struggle to adapt to these disturbances in real-time, compromising the overall performance and reliability of WEC systems. To address these challenges, an adaptive mechanism is employed in this study to fine-tune the controller parameters, thereby minimizing the impact of disturbances while guaranteeing system stability. Specifically, the Hamilton–Jacobi-Bellman theory is leveraged to establish a set of necessary and sufficient conditions, the solution to which dictates the adjustment of control law parameters. Typically, optimal control mechanisms necessitate knowledge of the signal history, including past disturbances, which can violate the causality of the physical system. To mitigate this limitation, a forecasting mechanism is incorporated into the control strategy. This mechanism is based on a NAR neural network, enabling to forecasting of the future behavior of external disturbance forces with higher accuracy. Its effectiveness is improved by integrating this forecasting capability into the control framework. This means that the controller can anticipate upcoming disturbances more precisely, allowing for proactive adjustments to maintain stability and optimize performance in dynamic ocean conditions.

Linear quadratic regulation (LQR), widely employed in various industrial contexts, addresses the linear quadratic optimization problem effectively. It boasts straightforward implementation and offers the benefits of reduced computational requirements and increased efficiency. Nevertheless, LQR is unable to handle the inherent disturbances and uncertainties present in the system. Given that a mathematical model of the WEC is derived from the linear potential flow theory analysis, there exists an alternative to the identification approach. Instead, the proposed controller can effectively manage the variations in the system parameters. This approach eliminates the need for explicit parameter identification and adaptation, as the controller is designed to dynamically adjust to changes in system characteristics. Therefore, by utilizing the inherent capabilities of the controller to adapt to varying parameters, the system can maintain robust performance without relying on explicit parameter identification techniques. Discovering the best controller parameter values can be accomplished through different approaches. For instance, in [41], a direct transcription method is presented, inherently relying on numerical techniques. In the proposed method, an analytical approach is developed based on a system of coupled ODEs, leading to a straightforward solution.

The methodology employed in this study involves several key components (Fig. 1). A detailed methodology for implementing the proposed adaptive optimal control strategy is presented, encompassing the considered single-body heaving point absorber WEC system description, mathematical representation of the WEC dynamics, and the generation mechanism of WEC reference velocities to track by the controller. The core of the proposed framework lies in integrating a NAR neural network for forecasting wave elevations and generating optimal reference velocities tailored to the specific characteristics of the WEC under consideration. Subsequently, the performance of the control strategy is analyzed through frequency and time domain response analysis, focusing on selected sea states representative of real-world conditions of two different selected locations near the Finland marine area. Additionally, the adaptability and robustness of the proposed approach are evaluated concerning variations in WEC dynamics, providing insights into its practical applicability and effectiveness.

This study addresses the dynamic challenges in WEC control through an adaptive optimal disturbance rejection framework. Unlike simpler feedforward or PID controllers that might struggle with system uncertainties and dynamic changes, the proposed approach provides a theoretically robust solution that can simultaneously track a performance-optimized reference and mitigate the effects of environmental disturbances. The methodology integrates a forecasting mechanism with a control law derived from the HJB theory, enabling the controller to proactively adjust to varying wave conditions and internal WEC dynamics. This combined approach of disturbance forecasting and optimal control is crucial for maintaining high efficiency and stability in the unpredictable marine environment. This research, therefore, focuses on demonstrating the efficacy of this advanced control framework, especially in scenarios involving a priori unknown variations in system dynamics.

The study proceeds as follows. Section 2 outlines the characteristics of the point absorber WEC under consideration, along with its equation of motion represented in state-space form. The details of the proposed control strategy are introduced in Section 3. Sections 4 and 5 describe the structure of the NAR network and generating the WEC reference velocities based on the forecasted sea surface wave elevation time series, respectively. The real wave climate data of the studied area for performance evaluation of the proposed control strategy is introduced in Section 6. The comprehensive evaluations of the proposed control strategy across different sea states and WEC dynamics variations are presented in Section 7. Finally, the conclusions of this research are provided in Section 8.

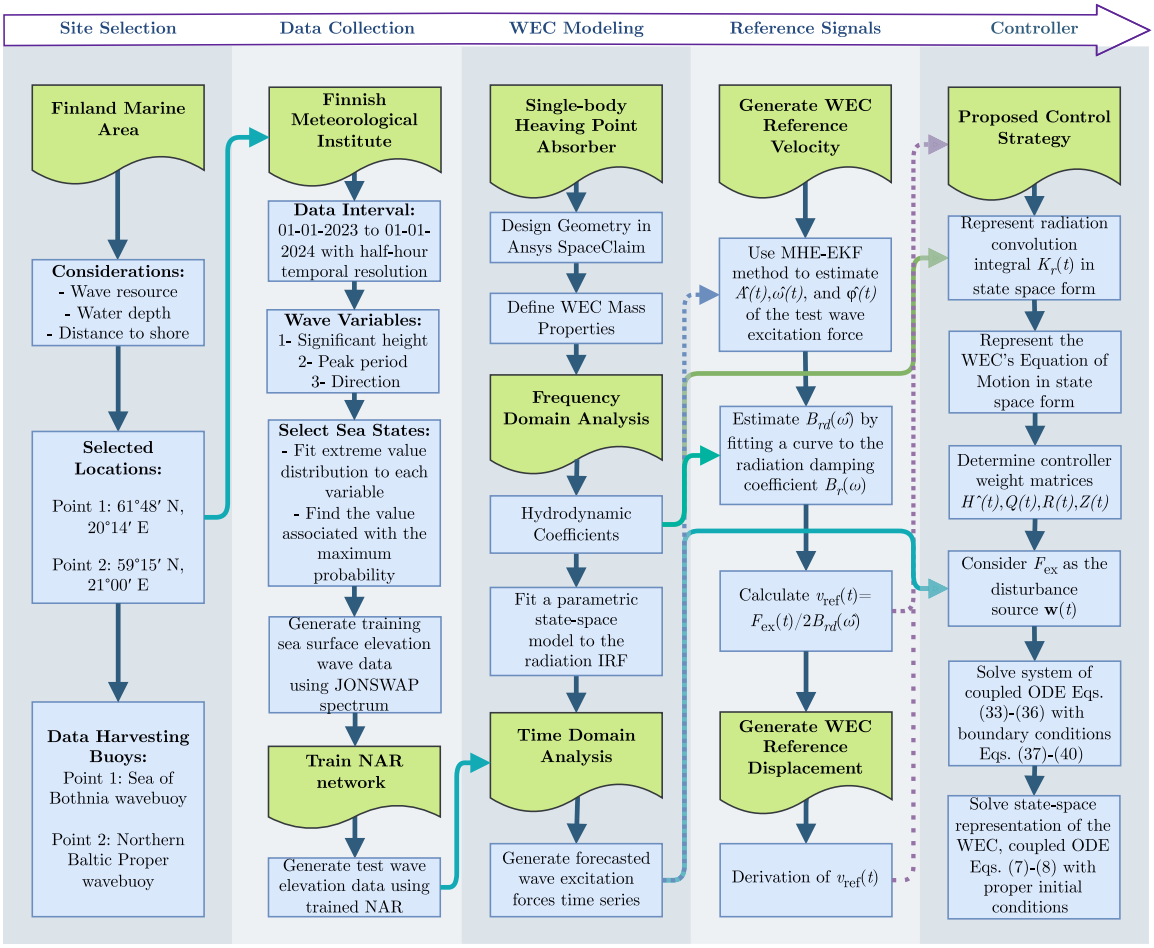

Fig. 1. Diagram of the considered methodology.

2. System description

2.1. Considered point absorber WEC

This study focuses on analyzing the performance of a single-body heaving point absorber WEC by applying the proposed control strategy. Point absorbers are recognized for their capability to efficiently harness energy across diverse oceanic conditions. Overall, point absorber WECs offer a promising path for renewable energy generation, combining efficiency, reliability, and environmental sustainability in harnessing the power of ocean waves. Fig. 2 presents a schematic diagram of the considered WEC. The structure of the floating body comprises an integrated cylinder and a hemisphere, rigidly interconnected to form a cohesive unit. The combined cylindrical and hemispherical geometry optimizes energy capture and stability. The hemispherical bottom enhances stability by lowering the center of buoyancy, while the cylindrical upper part improves energy absorption by amplifying the vertical motion response to wave excitation. The WEC device is coupled with a PTO system tethered to the seabed. Various PTO systems, such as hydraulic mechanisms and linear generators, can be employed to convert the mechanical energy derived from the heaving motion into electrical power. Table 1 outlines dimensional parameters and mass characteristics of the considered WEC. The parameter values listed in this table are based on the common dimensions and properties of point absorber designs documented in relevant wave energy converter research. The volumetric displacement and mass are derived from buoyancy and equilibrium considerations according to the selected geometry. These values are calculated to reflect realistic physical characteristics and to align with established models of similar WEC systems.

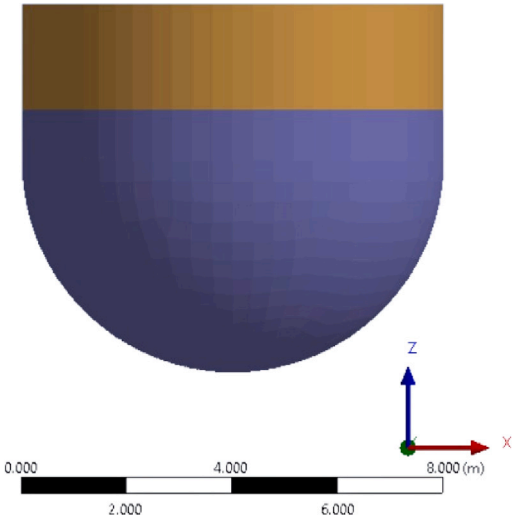

Fig. 2. Schematic diagram of the considered heaving point absorber WEC.

2.2. WEC equation of motion

The linear potential flow theory is employed to analyze the interaction between waves and structure. Linear potential flow theory simplifies the analysis by neglecting nonlinear effects such as viscous damping and wave breaking. While this assumption is suitable for mild

Table 1
The dimensions and mass properties of the considered point absorber WEC.

Parameter	Value	Unit
Cylinder diameter	8	m
Cylinder height	3	m
Hemisphere radius	4	m
Draught	5	m
Center of gravity (CoG) position concerning the global axis	$x = 0, y = 0, z = -2.4995$	m
Center of buoyancy (CoB) position concerning the global axis	$x = 0, y = 0, z = -1.9500$	m
Body mass	188 914.4382	kg
Volumetric displacement	184.3068	m^3
Moment of inertia around the x-axis (I_{xx})	1633662.6082	$kg.m^2$
Moment of inertia around the y-axis (I_{yy})	1633662.6082	$kg.m^2$
Moment of inertia around the z-axis (I_{zz})	1209132.8295	$kg.m^2$

wave conditions, it may lead to inaccuracies in highly nonlinear environments. Incorporating nonlinear hydrodynamic effects could provide a more realistic model but would necessitate a more complex controller to handle the additional dynamics and stronger disturbances.

The time-domain equation of motion of a single-body WEC in the heave direction can be expressed as [42]:

$$\left(m + m_\infty\right)\ddot{z}(t) + \int_0^t K_r(t-\tau)\dot{z}(\tau)\mathrm{d}\tau + k_{\mathrm{hs}} z(t) + c_v\dot{z}(t) = F_{\mathrm{ex}}(t) + F_{\mathrm{PTO}}(t) \quad (1)$$

here, m and m_∞ denote the mass and infinity added mass of the body, respectively. $z(t)$ represents the vertical displacement of the body's CoG at time t, while $\dot{z}$ and $\ddot{z}$ denote its velocity and acceleration, respectively. k_{hs} represents the hydrostatic restoring force given by $k_{hs} = \rho g s$, where ρ, g, and s are the seawater density, gravitational acceleration, and body cross-sectional area, respectively. The term $c_v\dot{z}(t)$ accounts for linear viscous damping with c_v being the damping coefficient. F_{PTO} stands for the force generated by the PTO system, which can be optimized by the controller to maximize power performance. K_r represents the radiation impulse response function (IRF):

$$K_r(t) = \frac{2}{\pi}\int_0^\infty B_{rd}(\omega)\cos(\omega t)\mathrm{d}\omega \quad (2)$$

where, ω and $B_{rd}(\omega)$ stand for frequency and frequency-dependent radiation damping coefficient, respectively.

The term F_{ex} refers to the wave excitation force, accounting for the interaction between the body fixed at its equilibrium position and ocean waves [43]. This force arises from the varying water surface elevations and fluid pressures associated with the waves. The external force F_{ex} is determined by convolving the wave elevation $\eta(t)$ with the non-causal excitation IRF $K_{\mathrm{ex}}(t)$ [33]:

$$F_{\mathrm{ex}}(t) = \int_{-\infty}^{\infty} K_{\mathrm{ex}}(t-\tau)\,\eta(\tau)\,\mathrm{d}\tau \quad (3)$$

where, $K_{\mathrm{ex}}(t)$ is given by:

$$K_{\mathrm{ex}}(t) = \frac{1}{2\pi}\int_{-\infty}^{\infty} X(\omega,\beta)\,e^{i\omega t}\mathrm{d}\omega \quad (4)$$

here, β represents the incident wave direction and $X(\cdot,\cdot)$ denotes the excitation force magnitude.

It should be noted that, within linear potential flow theory, the wave excitation force can be represented in multiple mathematically equivalent forms. The most common are: (i) a summation of harmonic components obtained from the wave spectrum, and (ii) a time-domain convolution between the wave elevation and the excitation impulse response function. In the present study, a compact parametric formulation is adopted in which the excitation force is computed directly from the predicted wave elevation using precomputed frequency-dependent excitation coefficients obtained from Ansys. This representation is equivalent in physical content to the convolution form but is more convenient for integration with the optimal control framework, as it bypasses the explicit convolution step while preserving the hydrodynamic accuracy of the model.

The radiation impulse response function ($K_r(t)$) and the frequency-dependent added mass ($A(\omega)$) are used to calculate the infinite frequency added mass (m_∞). The calculation is based on the relationship:

$$m_\infty = A(\omega) + \frac{1}{\omega}\int_0^\infty K_r(t)\sin(\omega t)\,dt \quad (5)$$

This equation is implemented numerically by evaluating the integral over time t for each frequency and averaging the results across the considered frequency range.

2.3. State-space representation of WEC's equation of motion

The state-space representation of the equation of motion is widely adopted in the design of WECs' control systems. This approach offers computational advantages by simplifying the calculation of the convolution integral within the radiation force equation, leading to improved computational speed [44]. To address the challenge of the convolution integral of the radiation force term, an approximation can be made using a state-space method, as depicted below:

$$\begin{aligned}\dot{\mathbf{x}}_r(t) &= A_r\mathbf{x}_r(t) + B_r\dot{z}(t)\\ y_r(t) &= C_r\mathbf{x}_r(t) \approx \int_0^t K_r(t-\tau)\dot{z}(\tau)\mathrm{d}\tau\end{aligned} \quad (6)$$

where $K_r(t) = C_r e^{A_r t} B_r$. Here, the state matrix ($A_r \in \mathbb{R}^{n_r\times n_r}$) governs the dynamics of the state vector $\mathbf{x}_r$ over time, the input matrix ($B_r \in \mathbb{R}^{n_r\times 1}$) maps the heave velocity $\dot{z}(t)$ to the state vector, the output matrix ($C_r \in \mathbb{R}^{1\times n_r}$), which relates the state vector $\mathbf{x}_r$ to the output y_r, the state vector ($\mathbf{x}_r \in \mathbb{R}^{n_r\times 1}$) represents the time history of the radiation force kernel. The parameter n_r represents the number of states used to approximate the convolution integral, which is chosen based on the desired level of accuracy. The common method for deriving the realization involves applying a Singular Value Decomposition (SVD) on the Hankel matrix associated with the impulse response function [45,46], which is utilized in this study. Therefore, the equation of motion of a single-body heaving point absorber WEC, denoted as Eq. (1), can be reformulated into a generalized state-space representation as follows

$$A = \begin{bmatrix} 0 & 1 & [0]_{1\times n_r} \\ -\frac{k_{hs}}{m+m_\infty} & -\frac{c_v}{m+m_\infty} & -\frac{c_r}{m+m_\infty} \\ [0]_{n_r\times 1} & B_r & A_r \end{bmatrix}, B = \begin{bmatrix} 0 \\ \frac{1}{m+m_\infty} \\ [0]_{n_r\times 1} \end{bmatrix},$$
$$C = \begin{bmatrix} 1 & 0 & [0]_{1\times n_r} \\ 0 & 1 & [0]_{1\times n_r} \end{bmatrix}, D = \begin{bmatrix} 0 \\ 0 \end{bmatrix} \quad (7)$$

3. Proposed control strategy

The block diagram of the proposed control strategy is depicted in Fig. 3. Consider the given state-space representation of the WEC:

$$\dot{\mathbf{x}}(t) = A(t)\mathbf{x} + B(t)\mathbf{u} + \mathbf{w}(t) \quad (8)$$

$$\mathbf{y}(t) = C(t)\mathbf{x} \quad (9)$$

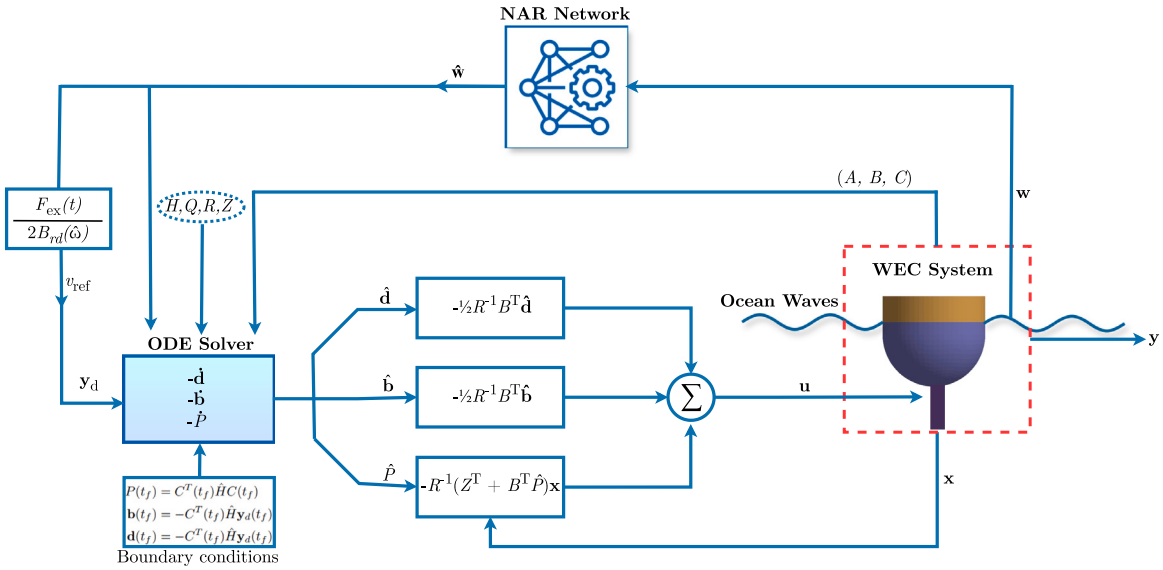

Fig. 3. Block diagram of the proposed control strategy.

here, $\mathbf{u}(\cdot)$ represents the control input of the PTO system, and $\mathbf{w}(\cdot)$ is the disturbance input. In this study, the wave excitation force is considered as the external disturbance influencing the considered WEC. The output signal $\mathbf{y}(\cdot)$ is of particular interest as it is desired to track a reference signal $\mathbf{y}_d(\cdot)$ such as WEC velocity to make resonance in the system. By achieving resonance, the heaving point absorber can efficiently capture and convert wave energy into electrical power, maximizing its energy output and effectiveness. The goal is to adjust the control input $\mathbf{u}$ in such a way that the output signal $\mathbf{y}$ tracks the desired reference signal $\mathbf{y}_d$. The performance index is:

$$J(\mathbf{x}_0,\mathbf{u})=\mathbf{e}^T(t_f)\hat{H}\mathbf{e}(t_f)+\int_{t_0}^{t_f}\Big(\mathbf{e}^T(t)Q(t)\mathbf{e}(t)+\mathbf{u}^T(t)R(t)\mathbf{u}(t)+2\mathbf{x}^T(t)Z(t)\mathbf{u}(t)\Big)dt \quad (10)$$

where $\mathbf{e}(t)=\mathbf{y}(t)-\mathbf{y}_d(t)$ is the difference between the actual output and its desired value. The terminal cost, i.e., the term outside of the integral in Eq. (10) can be expanded as follows:

$$\mathbf{e}^T(t_f)\hat{H}\mathbf{e}(t_f)=\big(C(t_f)\mathbf{x}(t_f)-\mathbf{y}_d(t_f)\big)^T\hat{H}\big(C(t_f)\mathbf{x}(t_f)-\mathbf{y}_d(t_f)\big) \quad (11)$$

$$=\mathbf{x}^T(t_f)C^T(t_f)\hat{H}C(t_f)\mathbf{x}(t_f)-2\mathbf{y}_d^T(t_f)\hat{H}C(t_f)\mathbf{x}(t_f)+\mathbf{y}_d^T(t_f)\hat{H}\mathbf{y}_d(t_f) \quad (12)$$

The expression includes both quadratic and linear components of $\mathbf{x}(t_f)$, along with an additional unrelated term involving it. By expanding the integrand terms in Eq. (10):

$$\big(C(t)\mathbf{x}(t)-\mathbf{y}_d(t)\big)^TQ(t)\big(C(t)\mathbf{x}(t)-\mathbf{y}_d(t)\big)+\mathbf{u}^T(t)R(t)\mathbf{u}(t)+2\mathbf{x}^T(t)Z(t)\mathbf{u}(t) \quad (13)$$

$$=\mathbf{x}^T(t)C^T(t)Q(t)C(t)\mathbf{x}(t)-2\mathbf{y}_d^T(t)Q(t)C(t)\mathbf{x}(t)+\mathbf{u}^T(t)R(t)\mathbf{u}(t) \quad (14)$$

$$+2\mathbf{x}^T(t)Z(t)\mathbf{u}(t)+\mathbf{y}_d^T(t)Q(t)\mathbf{y}_d(t) \quad (15)$$

The Hamlitonian function can be defined as follows by considering $V(\mathbf{x},t)$ as the optimal value of $J(\mathbf{x},t)$

$$\mathcal{H}=\mathbf{x}^T(t)C^T(t)Q(t)C(t)\mathbf{x}(t)-2\mathbf{y}_d^T(t)Q(t)C(t)\mathbf{x}(t)+\mathbf{u}^T(t)R(t)\mathbf{u}(t)$$
$$+2\mathbf{x}^T(t)Z(t)\mathbf{u}(t)+\mathbf{y}_d^T(t)Q(t)\mathbf{y}_d(t)+\Big(\frac{\partial V}{\partial\mathbf{x}}\Big)^T\Big(A(t)\mathbf{x}+B(t)\mathbf{u}+\mathbf{w}(t)\Big) \quad (16)$$

The minimum of $\mathcal{H}$ with respect to the control signal $\mathbf{u}$ can be found by setting $\mathcal{H}_{\mathbf{u}}$ to zero

$$\frac{\partial\mathcal{H}}{\partial\mathbf{u}}=2R(t)\mathbf{u}+2Z^T(t)\mathbf{x}+B^T(t)\Big(\frac{\partial V}{\partial\mathbf{x}}\Big)=0 \quad (17)$$

which results in

$$\hat{\mathbf{u}}=-\frac{1}{2}R^{-1}(t)\Big(2Z^T(t)\mathbf{x}+B^T(t)\Big(\frac{\partial V}{\partial\mathbf{x}}\Big)\Big) \quad (18)$$

By substituting the minimizer signal, $\hat{\mathbf{u}}$, in the Hamiltonian of Eq. (16), it yields

$$\mathcal{H}_{min}=\mathbf{x}^T(t)C^T(t)Q(t)C(t)\mathbf{x}(t)-2\mathbf{y}_d^T(t)Q(t)C(t)\mathbf{x}(t)+\hat{\mathbf{u}}^T(t)R(t)\hat{\mathbf{u}}(t) \quad (19)$$

$$+2\mathbf{x}^T(t)Z(t)\hat{\mathbf{u}}(t)+\mathbf{y}_d^T(t)Q(t)\mathbf{y}_d(t)+\Big(\frac{\partial V}{\partial\mathbf{x}}\Big)^T\Big(A(t)\mathbf{x}+B\hat{\mathbf{u}}+\mathbf{w}(t)\Big) \quad (20)$$

$$=\mathbf{x}^T(t)\Big(C^T(t)Q(t)C(t)-Z(t)R^{-1}(t)Z^T(t)\Big)\mathbf{x}(t) \quad (21)$$

$$+\mathbf{x}^T(t)\Big(-2C^T(t)Q(t)\mathbf{y}_d(t)+A^T\Big(\frac{\partial V}{\partial\mathbf{x}}\Big)-Z(t)R^{-1}(t)B^T(t)\Big(\frac{\partial V}{\partial\mathbf{x}}\Big)\Big) \quad (22)$$

$$+\mathbf{y}_d^T(t)Q(t)\mathbf{y}_d(t)+\Big(\frac{\partial V}{\partial\mathbf{x}}\Big)^T\mathbf{w}(t)-\frac{1}{4}\Big(\frac{\partial V}{\partial\mathbf{x}}\Big)^TB(t)R^{-1}(t)B^T(t)\Big(\frac{\partial V}{\partial\mathbf{x}}\Big) \quad (23)$$

To solve the Hamilton–Jacobi-Bellman (HJB) equation, the following form can be selected with undetermined coefficients

$$V(\mathbf{x},t)=\mathbf{x}^TP(t)\mathbf{x}+\big(\mathbf{b}(t)+\mathbf{d}(t)\big)^T\mathbf{x}+\upsilon(t) \quad (24)$$

in which $P(\cdot)\in\mathbb{R}^{n\times n}$, $\mathbf{b}(\cdot),\mathbf{d}(\cdot)\in\mathbb{R}^{n\times1}$, and $\upsilon(\cdot)\in\mathbb{R}$ must be computed. Without loss of generality, it is assumed $P(t)=P^T(t)\geq0$. The quadratic form assumption for the value function simplifies the solution of the HJB equation which makes it computationally feasible for real-time control applications. However, in highly nonlinear systems or with non-quadratic cost functions, this approximation may result in suboptimal control performance.

Recalling the HJB equation, i.e.,

$$-\frac{\partial V}{\partial t}=\min\mathcal{H} \quad (25)$$

one can obtain the following in which the argument t is omitted for simplifying the notation

$$-\mathbf{x}\dot{P}\mathbf{x}-\mathbf{x}^T(\dot{\mathbf{b}}+\dot{\mathbf{d}})-\dot{\upsilon}=\mathbf{x}^T\Big(C^TQC-ZR^{-1}Z^T\Big)\mathbf{x} \quad (26)$$

$$+\mathbf{x}^T\Big(-2C^TQ\mathbf{y}_d+A^T(2P\mathbf{x}+\mathbf{b}+\mathbf{d}) \quad (27)$$

$$-ZR^{-1}B^T(2P\mathbf{x}+\mathbf{b}+\mathbf{d})\Big) \quad (28)$$

$$+\mathbf{y}_d^TQ\mathbf{y}_d+\big(2P\mathbf{x}+\mathbf{b}+\mathbf{d}\big)^T\mathbf{w} \quad (29)$$

$$-\frac{1}{4}\big(2P\mathbf{x}+\mathbf{b}+\mathbf{d}\big)^TBR^{-1}B^T\big(2P\mathbf{x}+\mathbf{b}+\mathbf{d}\big) \quad (30)$$

which can be simplified as

$$\mathbf{x}^T\Big(C^TQC-ZR^{-1}Z^T+2A^TP-2ZR^{-1}B^TP-P^TBR^{-1}B^TP\Big)\mathbf{x} \quad (31)$$

$$+ \mathbf{x}^T\left(-2C^TQ\mathbf{y}_d + A^T(\mathbf{b}+\mathbf{d}) - ZR^{-1}B^T(\mathbf{b}+\mathbf{d}) + 2P\mathbf{w} - P^TBR^{-1}B^T(\mathbf{b}+\mathbf{d})\right) \tag{32}$$

$$+ \mathbf{y}_d^TQ\mathbf{y}_d + (\mathbf{b}+\mathbf{d})^T\mathbf{w} - \frac{1}{4}(\mathbf{b}+\mathbf{d})^TBR^{-1}B^T(\mathbf{b}+\mathbf{d}) \tag{33}$$

which sequentially results in

$$-\dot{P} = A^TP + PA + C^TQC - ZR^{-1}Z^T - 2ZR^{-1}B^TP - P^TBR^{-1}B^TP \tag{34}$$

$$-\dot{\mathbf{b}} = \left(A - BR^{-1}Z^T - BR^{-1}B^TP\right)^T\mathbf{b} - 2C^TQ\mathbf{y}_d \tag{35}$$

$$-\dot{\mathbf{d}} = \left(A - BR^{-1}Z^T - BR^{-1}B^TP\right)^T\mathbf{d} + 2P\mathbf{w} \tag{36}$$

$$-\dot{v} = \mathbf{y}_d^TQ\mathbf{y}_d + 2\mathbf{b}^T\mathbf{w} - \frac{1}{4}(\mathbf{b}+\mathbf{d})^TBR^{-1}B^T(\mathbf{b}+\mathbf{d}) \tag{37}$$

Considering $V(\mathbf{x}(t_f), t_f)$ as $\mathbf{e}^T(t_f)\hat{H}\mathbf{e}(t_f)$, the following boundary conditions are found

$$P(t_f) = C^T(t_f)\hat{H}C(t_f) \tag{38}$$

$$\mathbf{b}(t_f) = -C^T(t_f)\hat{H}\mathbf{y}_d(t_f) \tag{39}$$

$$\mathbf{d}(t_f) = -C^T(t_f)\hat{H}\mathbf{y}_d(t_f) \tag{40}$$

$$v(t_f) = \mathbf{y}_d^T(t_f)\hat{H}\mathbf{y}_d(t_f) \tag{41}$$

Solving the equations yields the optimal control obtained in Eq. (18) as

$$\mathbf{u}^o(\mathbf{x},t) = -R^{-1}\left(Z^T(t) + B^T(t)P(t)\right)\mathbf{x} - \frac{1}{2}R^{-1}B^T(t)\left(\mathbf{b}(t)+\mathbf{d}(t)\right) \tag{42}$$

which is composed of two terms: the former is responsible for the stability of the closed-loop and the latter compensates the disturbance and solves the tracking issue.

As can be seen from these results, the differential equations must be solved sequentially: $P \rightarrow \mathbf{b} \rightarrow v$. The main concern is that for solving $\mathbf{b}(t)$ the disturbance input over (t, t_f) is needed which means the structure of the control is not causal. Of course, if $\mathbf{w}(t)$ is indeed known for all time steps, the signal $R^{-1}(t)B^T(t)\mathbf{b}(t)$ can be computed offline. One solution is modeling the disturbance signal by a high-order state space dynamic, e.g., a linear filter whose parameters are already known. Another way is estimating/forecasting the behavior of the disturbance and utilizing it in the design process. Here, the NAR neural network is used to forecast the wave elevation time series and subsequently estimate the wave excitation force, as the disturbance signal, during the duration over which the control algorithm operates. In practical implementation, real-time feedback mechanisms face challenges such as environmental fluctuations. The proposed control strategy accounts for such issues. Additionally, the controller is designed to adjust for varying wave conditions, ensuring stable performance in dynamic marine environments.

It is important to clarify that although the excitation force $F_{\text{ex}}(t)$ is referred to as a 'disturbance' within the optimal disturbance rejection framework, it is not being rejected in the traditional sense of disturbance attenuation. In fact, it represents the primary source of energy to be harvested by the WEC. The proposed strategy does not aim to suppress or eliminate this input. Instead, it anticipates the excitation force using a NAR neural network and generates an optimal reference velocity that is in phase with $F_{\text{ex}}(t)$, as per Eq. (48) [47]. This phase alignment maximizes the instantaneous absorbed power. Hence, the control problem is still fundamentally energy-maximizing. The terminology of 'disturbance rejection' used here aligns with the control-theoretic structure adopted for solving the HJB-based tracking problem but does not imply a mischaracterization of $F_{\text{ex}}(t)$. Moreover, the term $2\mathbf{x}^T(t)Z(t)\mathbf{u}(t)$ in the performance index, Eq. (10), is directly responsible for promoting energy absorption by the WEC. In the WEC systems, the absorbed power is typically calculated as the product of the PTO force and the heave velocity of the device. Since the state vector $\mathbf{x}(t)$ includes the heave velocity component and the control input $\mathbf{u}(t)$ corresponds to the PTO force, this cross-term in the cost function explicitly encourages the controller to align the velocity and force in phase. This alignment is known to maximize the instantaneous absorbed power. Thus, although the performance index contains tracking and effort penalization terms, the inclusion of the $\mathbf{x}^TZ\mathbf{u}$ term inherently formulates the control problem with an energy-maximizing objective. This approach guarantees that the proposed controller is consistent with the physical goal of maximizing energy extraction from ocean waves.

4. Nonlinear autoregressive neural network

A NAR network is a type of recurrent dynamic network [48] used for time series forecasting according to its ability to capture the nonlinear patterns in time series data. Ocean waves exhibit nonlinear characteristics, especially under the influence of varying wind speeds and directions, changing seabed topography, and interactions with other waves. NAR network can capture these nonlinear dynamics effectively. NAR network, with its recurrent structure, can learn from historical wave data and recognize temporal patterns and dependencies, which are crucial for accurate wave forecasting. It can adapt to new patterns in wave data, making it robust to changes in wave behavior over time.

The NAR network can make multi-step-ahead forecasting, which is essential for WEC control purposes. The network uses feedback connections from previous outputs as part of the input for the next step. In general, the NAR network can be expressed as [33]

$$\hat{y}(t) = f\left(y(t-1) + y(t-2) + \cdots + y(t-k)\right) \tag{43}$$

Here, f denotes the mapping function learned by the neural network, $y(t)$ represents the historical value of the time series at time step t, $\hat{y}(t)$ is the forecasted output at time step t, and k signifies the length of the lag window.

A general schematic diagram of a NAR neural network architecture with two hidden layers is shown in Fig. 4. The structure of a NAR network typically consists of an input layer, hidden Layer/s, and an output layer [49]. The input layer consists of the historical time series data, which the network uses to make predictions. One or more hidden layers can be used which are responsible for capturing the nonlinear relationships within the data. Hidden layers can contain multiple neurons which are crucial for the network's ability to learn and make predictions [50]. Each neuron in these layers applies a nonlinear activation function (such as sigmoid, tanh, or ReLU) to the weighted sum of its inputs [51]. The output layer is the last layer of the NAR structure that produces the predictions. Connecting the network layers is associated with weights and biases that the network should learn and find their optimum values during the training process [52]. Weights determine the strength of the connection between neurons, and biases allow the activation function to be shifted. The training process consists of adjusting the weights and biases of the network to minimize the difference between the predicted and actual values using an optimization algorithm such as the gradient descent method [53,54]. Thoroughly adjusting parameters and refining training strategies is vital to prevent overfitting and achieve better performance. Feedback connections are connections from the output layer back to the input or hidden layers, allowing it to use past predicted values as input for future predictions.

5. Generating WEC reference velocity

To achieve the highest output power, it is crucial for the controller to accurately track a reference WEC velocity. This reference velocity can be derived from knowledge of the wave excitation force acting on the WEC body. In this study, a method introduced in previous works [55,56] is employed to generate the reference velocity. Assuming that the input signal $F_{\text{ex}}(t)$ exhibits narrowband harmonic characteristics, with varying parameters over time amplitude $\hat{A}(t)$, frequency $\hat{\omega}(t)$,

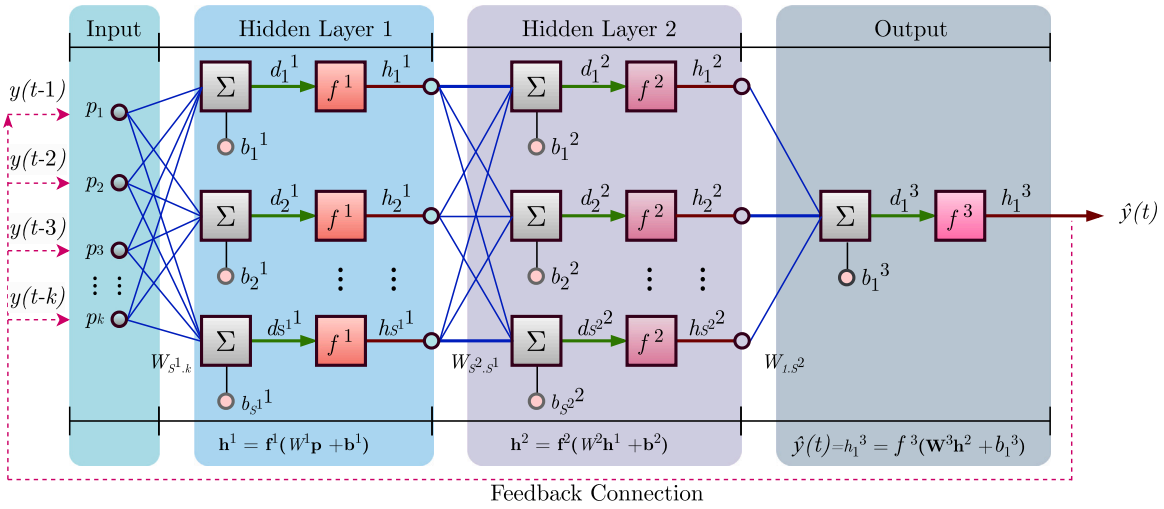

Fig. 4. A Schematic diagram of a NAR neural network with two hidden layers.

and phase $\hat{\varphi}(t)$:

$$\hat{F}_{ex}(t) = \hat{A}(t)\cos(\hat{\omega}(t)t + \hat{\varphi}(t)) \tag{44}$$

For real-time estimation of the unknown parameters of this equation, the Moving Horizon Estimation with Extended Kalman Filter (MHE-EKF) [57,58] is utilized. The state vector is defined as $\mathbf{x}(t) = [A(t),\ \omega(t),\ \varphi(t)]^{T}$. A random-walk process model is assumed for the parameter evolution:

$$\mathbf{x}_{k+1} = \mathbf{x}_k + \mathbf{w}_k, \tag{45}$$

where $\mathbf{w}_k$ is zero-mean Gaussian process noise with covariance $Q = \mathrm{diag}(10^{9},\ 10^{-9},\ 1)$. The measurement model relates the measured excitation force y_k to the state variables:

$$y_k = A_k\cos(\omega_k t_k + \varphi_k) + v_k, \tag{46}$$

with v_k zero-mean Gaussian noise of variance $R = 0.01$. The Jacobian of the measurement model with respect to $\mathbf{x}_k$ is computed analytically at each update step as

$$H_k = \begin{bmatrix}\cos(\omega_k t_k + \varphi_k) & -A_k t_k \sin(\omega_k t_k + \varphi_k) & -A_k \sin(\omega_k t_k + \varphi_k)\end{bmatrix}. \tag{47}$$

The reference velocity $v_{ref}(t)$ can then be generated using the equation

$$v_{ref}(t) = \frac{F_{ex}(t)}{2B_{rd}(\hat{\omega})} \tag{48}$$

here, $B_{rd}(\hat{\omega})$ is determined for each $\hat{\omega}$ by fitting a curve to the radiation damping coefficient B_{rd} and ω values.

It is worth noting that the generated reference velocity inherently aims to maximize the absorbed wave power, as it is directly proportional to the estimated excitation force $\hat{F}_{ex}(t)$, which appears in the absorbed power term $P_{abs}(t) = F_{ex}(t)\,\dot{z}(t)$. In this study, the reference velocity is obtained without explicit enforcement of actuator force limits, motion bounds, or PTO power caps, in order to evaluate the underlying forecasting and tracking components in an unconstrained setting. This simplification allows for isolating the contribution of the proposed MHE-EKF forecasting and control strategy to the overall performance. Nevertheless, the formulation can be readily extended to incorporate such physical constraints by embedding the reference profile generation into a constrained optimization framework (e.g., model predictive control), where the excitation force estimate serves as a predictive input.

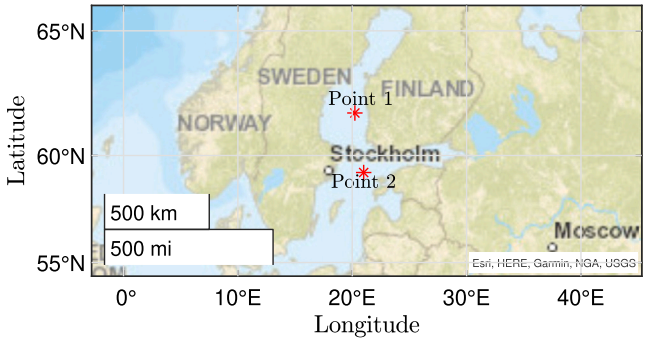

Fig. 5. The geographical location of the selected points to evaluate the performance of the proposed control theory.

6. Wave data

The performance of the proposed control strategy is evaluated based on the real wave climate of two selected locations around Finland. These points are chosen in the locations of Waverider wave buoys installed by the Finnish Meteorological Institute [59] which is a branch of the Ministry of Transport and Communications. The details of the selected locations are shown in Table 2. Moreover, Fig. 5 shows the geographical location of the selected points. The collected one-year half-hour temporal resolution significant wave height, wave peak period, and wave direction of these points are depicted in Fig. 6.

7. Results and discussion

7.1. Frequency domain response analysis

This study employs Ansys Aqwa, software based on linear potential flow theory, to simulate the hydrodynamic fluid wave loading on the WEC body in the frequency domain. Following analysis in the frequency domain and obtaining the hydrodynamic coefficients, they can be integrated into the WEC's time-domain equations of motion, represented as Eq. (1), enabling investigation into the dynamic response of the system under different irregular wave conditions. In the analyses, the origin of the global axis is located at the mean free surface, which constitutes a right-handed coordinate system. The vertical axis, denoted as Z-axis, extends upwards. The wave direction is the angle between the direction of propagation and the positive X-axis in an anti-clockwise manner.

Table 2
The details of selected points to evaluate the performance of the proposed control theory.

Location	Buoy	Coordinate	Water Depth (m)	Data Collection Interval
Point 1	Sea of Bothnia wavebuoy	61°48′ N, 20°14′ E	111	01-01-2023 to 01-01-2024
Point 2	Northern Baltic Proper wavebuoy	59°15′ N, 21°00′ E	105	01-01-2023 to 01-01-2024

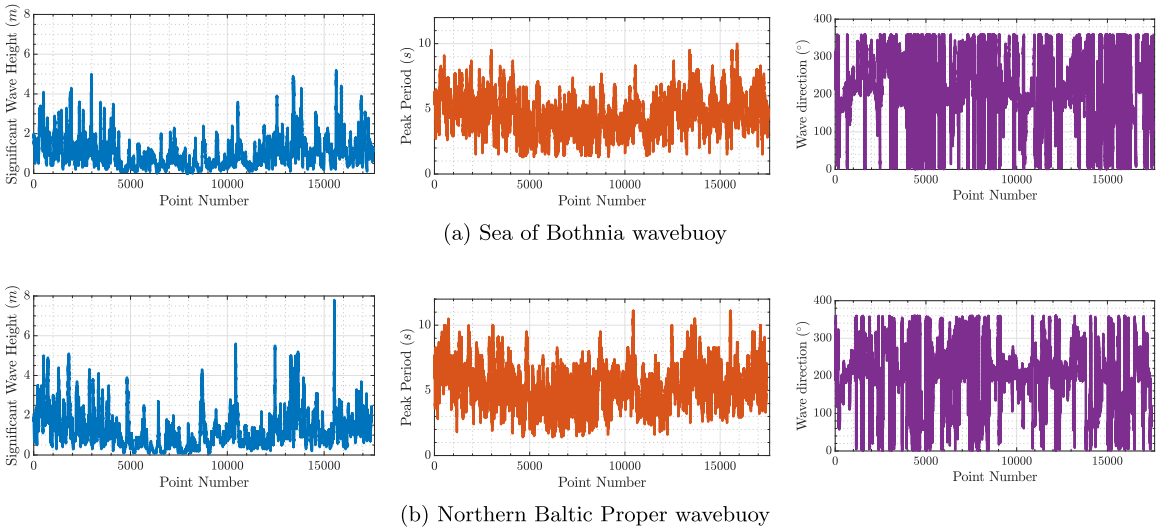

(a) Sea of Bothnia wavebuoy

(b) Northern Baltic Proper wavebuoy

Fig. 6. The collected one-year half-hour temporal resolution significant wave height, wave peak period, and wave direction of the selected points.

Table 3
Setup parameters for the frequency domain response analysis.

Parameter	Value	Unit
Water density, ρ	1025	kg m^{-3}
Wave directions, β	$-180, -120, -60, 0, 60, 120, 180$	degree
Gravitational acceleration, g	9.806	m s^{-2}
Frequency range, ω	0.1 to 3.5 with 40 steps	rad s^{-1}
Viscous force coefficient, c_v	0	N s/m^2

The mass properties of the floating body are detailed in Table 1. Other simulation parameters are shown in Table 3. Moreover, Fig. 7 shows the numerical mesh model of the considered WEC which is used for calculating hydrodynamic coefficients.

The results of the frequency domain hydrodynamic analysis of the considered WEC are presented in Fig. 8. This figure displays the added mass, radiation wave damping, excitation force phase and magnitude, excitation, and radiation IRFs. These IRFs are computed from $t = 0$ to 150 s. Additionally, a parametric state-space model fitted to the radiation IRF of order $n_r = 3$ is depicted. Furthermore, the values of the added mass at infinite frequency m_∞ and the linear hydrostatic restoring coefficient k_{hs} are determined as 75466.42 kg and 504220 N.m^{-1}, respectively.

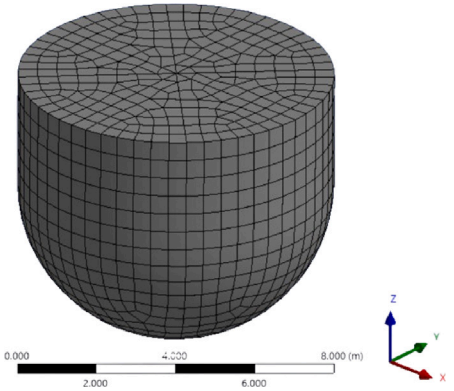

Fig. 7. Numerical mesh model of the considered heaving point absorber WEC used for calculating hydrodynamic coefficients.

7.2. Selected sea states of the studied points

It is needed to determine the sea state of the studied locations (see Table 2) in such a way that is representative of the wave climate in these points. These sea states are utilized for performance evaluation of the considered WEC model in the time domain. Since the selected locations have a calm wave climate in general, here the focus is on modeling extreme events of the wave climate for risk assessment and decision-making. To this purpose, Extreme value distribution is fitted to the wave data to model extreme events more accurately and to estimate the probability of such events occurring within a given dataset or period. The selection of an appropriate extreme value distribution is crucial for accurately predicting extreme wave events.

The histogram with fitted extreme value distribution to the collected one-year significant wave height, wave peak period, and wave direction of the selected points is illustrated in Fig. 9. Moreover, the details of the fitting results are shown in Table 4. The parameters μ and σ are the mean and standard deviation of the fitted distribution, respectively. The maximum probability and the value associated with the maximum probability are also presented in this table. The values associated with the maximum probabilities are chosen as the candidates for the sea states of the studied points. It should be noted that here the wave direction is not important because the considered WEC is a heaving point absorber type and can extract the wave power in different directions.

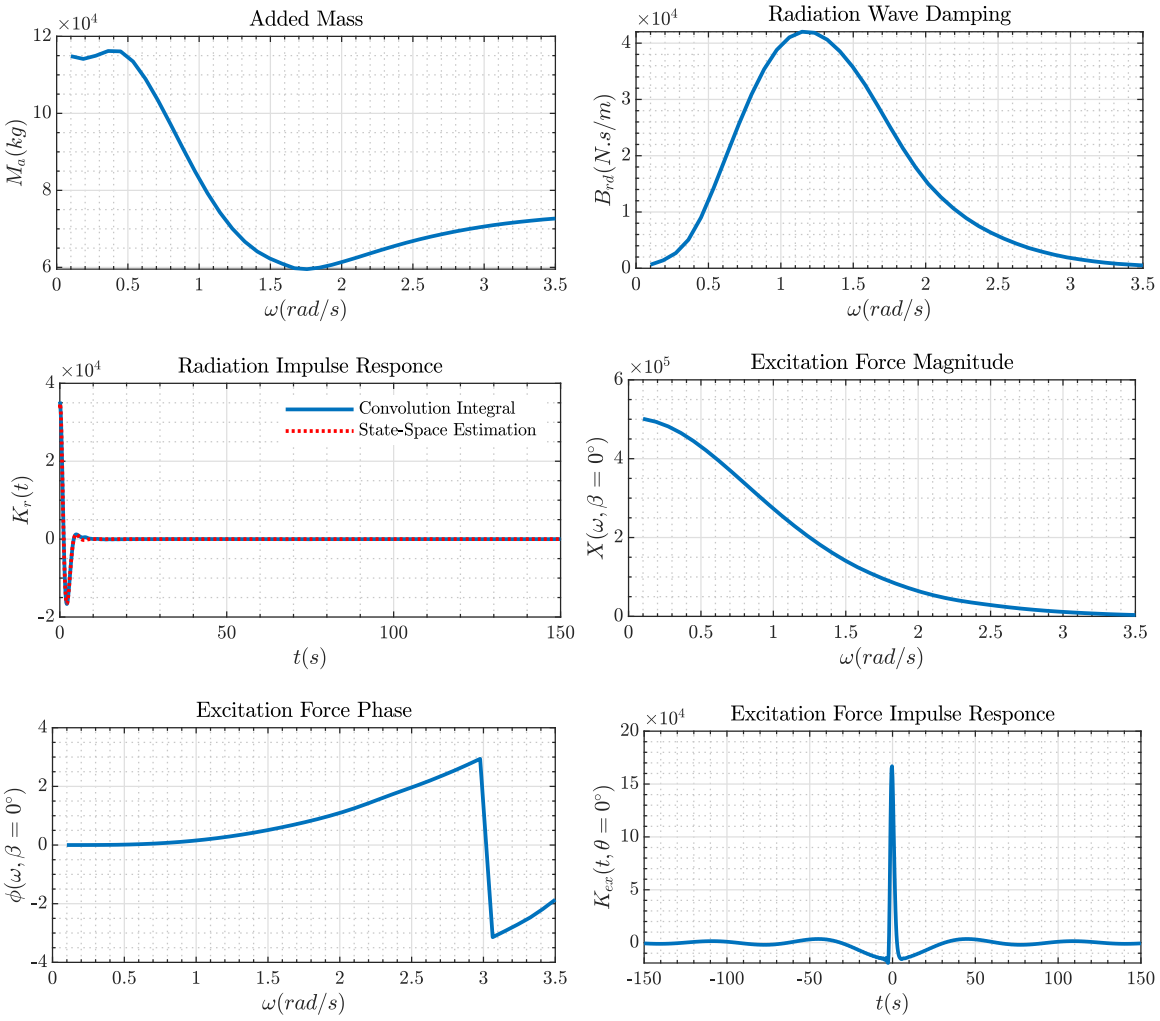

Fig. 8. Results of frequency domain hydrodynamic analysis of the considered heaving point absorber WEC.

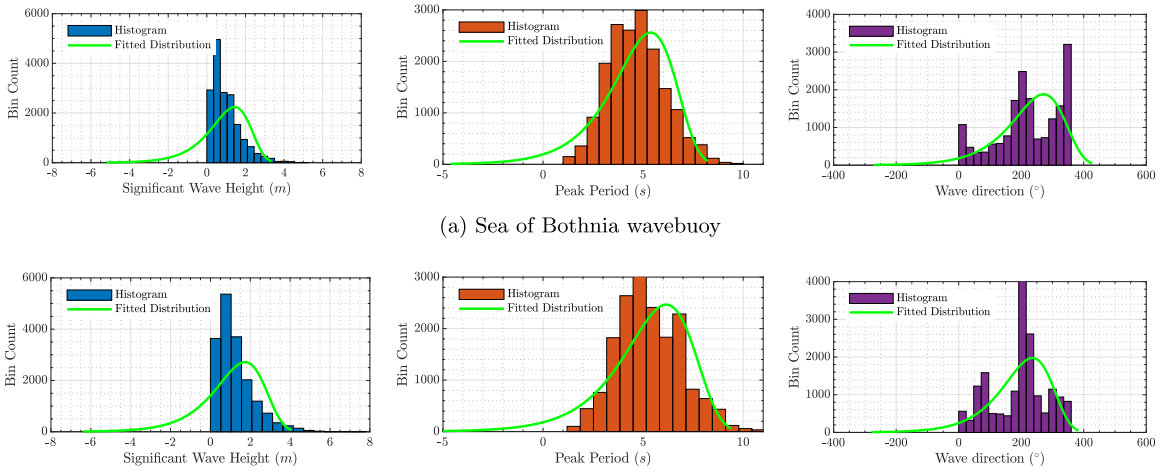

(a) Sea of Bothnia wavebuoy

(b) Northern Baltic Proper wavebuoy

Fig. 9. The histogram with fitted extreme value distribution to the collected one-year half-hour temporal resolution significant wave height, wave peak period, and wave direction of the selected points.

To model the disturbance signal (wave excitation force) in the studied locations, it is assumed that the 300 s wave elevation time series information is available before the start of the controller operation. Then, based on these past observations, it is possible to forecast the

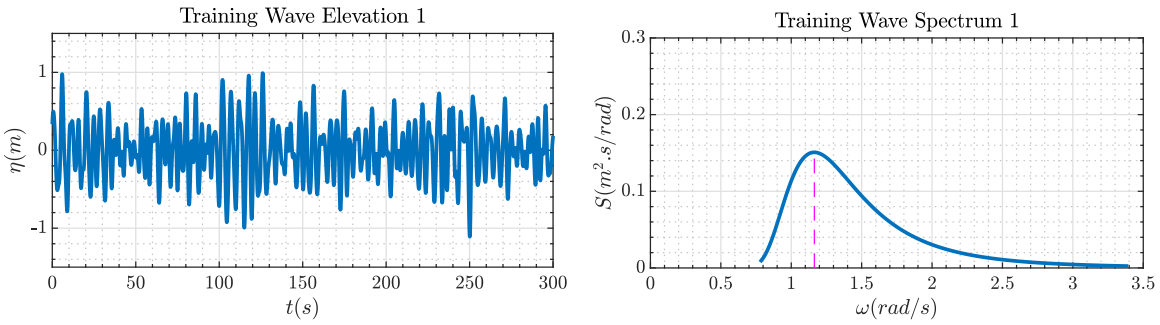

(a) Point 1, significant wave height $H_s = 1.4\ m$, peak period $T_p = 5.4\ s, \gamma = 1$

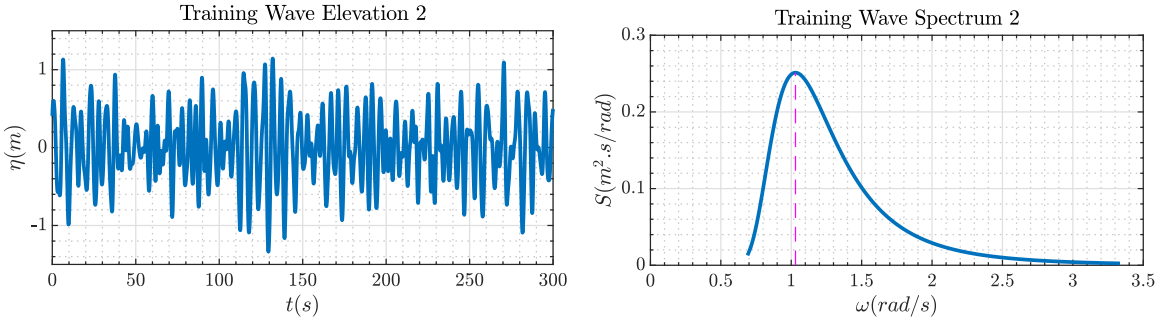

(b) Point 2, significant wave height $H_s = 1.7\ m$, peak period $T_p = 6.1\ s, \gamma = 1$

Fig. 10. The training irregular waves generated by the JONSWAP spectrum based on the sea states associated with the maximum probabilities of the selected points.

Table 4
Extreme value distribution fit results to the collected one-year half-hour temporal resolution significant wave height, wave peak period, and wave direction of the selected points.

Dataset	Variable	Max Prob	Value at Max Prob	μ	σ
Sea of	Significant Wave Height (m)	0.3648	1.4000	1.4396	1.0078
Bothnia	Wave Peak Period (s)	0.2432	5.4000	5.3830	1.5127
wavebuoy	Wave Direction (°)	0.0045	271	271.4683	82.3325
Northern Baltic	Significant Wave Height (m)	0.2992	1.7000	1.7356	1.2290
Proper	Wave Peak Period (s)	0.2141	6.1000	6.1589	1.7172
wavebuoy	Wave Direction (°)	0.0047	236	235.8649	77.9419

wave elevations using NAR network for future time steps. In the next step, the wave excitation force time series will be estimated based on the forecasted wave elevation time series which is needed by the controller to reject its effects. The training time series elevation of the generated waves and their JONSWAP spectrum are shown in Fig. 10. These wave elevation data are used to train the NAR network models to generate new wave elevations for performance evaluation of the proposed control strategy. The structural specifications of the developed NAR models for two selected points are outlined in Table 5. It is necessary to explain that these specifications are obtained after numerous network training to capture the best and most rational results for the training and forecasted sets. Fig. 11 displays the wave elevation time series comparison between the actual training data and the NAR model outputs. It is evident from the figure that the actual values closely match the forecasted values in both cases, indicating satisfactory accuracy for the training datasets. It is necessary to mention that while the NAR model provides accurate predictions under typical wave conditions, it may struggle to capture extreme wave events or highly irregular sea states due to limitations in training data or model generalization. To improve robustness in such scenarios, it is possible to explore incorporating a broader range of training data or using hybrid models that combine traditional forecasting methods with machine learning techniques to better handle rare, high-energy wave conditions. The 60 s ahead forecasted wave elevations and relevant wave excitation forces of the studied locations are depicted in Fig. 12. These two new waves are used to evaluate the performance of the proposed control strategy.

The observer mechanism is integral to the control strategy, continuously monitoring wave elevations over a defined period to capture the current wave environment. The NAR network is trained in real-time using the observed wave elevation data which enables the system to generate accurate forecasts tailored to immediate conditions. The proposed approach inherently adapts to different wave environments through the observer's tracking and the network's real-time training, obviating the need for pre-training on diverse datasets.

7.3. WEC reference velocities of the selected sea states

As mentioned in Section 5, the reference velocity v_{ref} is estimated based on Eq. (48) which specifies the WEC body oscillation velocity should be in phase with the wave excitation force. Fig. 13 shows the real-time estimations of the unknown parameters $\hat{A}(t)$, $\hat{\omega}(t)$, and $\hat{\varphi}(t)$ of Eq. (44) to estimate the wave excitation forces of the selected studied locations using MHE-EKF method. The MHE uses a horizon of $N = 5$ samples (0.5 s at the 10 Hz sampling rate), over which the EKF is applied iteratively to refine the parameter estimates. The initial state is set to $\mathbf{x}_0 = [0.1,\ 0.5,\ 1]^{\mathrm{T}}$ with initial covariance $P_0 = \mathrm{diag}(10^8,\ 0,\ 1)$. At each time step, the EKF processes the N most recent measurements

Table 5
The general structure details of the created NAR network models to forecast the wave elevations of the selected points.

Parameter	Value
Predictor and Response	Past observation time series of the wave elevation data
Number of feedback delays	200 (for Wave Elevation 1) and 30 (for Wave Elevation 2)
Number of layers	Two layers
Hidden Layer size	10
Hidden layer activation function	Hyperbolic tangent sigmoid
Output layer activation	None
Training data ratio	70% of the entire data set
Validation data ratio	15% of the entire data set
Test data ratio	15% of the entire data set
Layer biases initializer	Zeros
Update the network learnable parameters	Levenberg–Marquardt backpropagation
Minimum gradient	1e−7
Maximum validation checks	6
Mu	0.001
Performance function	Mean Square Error (MSE)
Performance Goal	0
Maximum number of epochs	1000

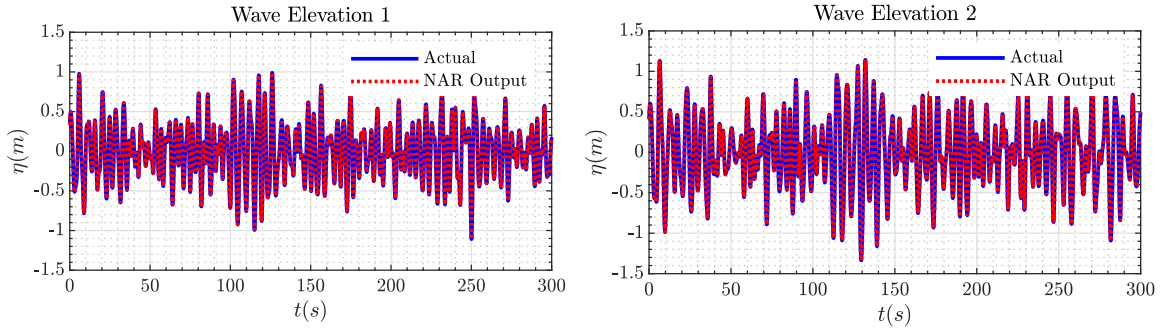

Fig. 11. Time series of the wave elevation training actual values vs. NAR network outputs of the selected points.

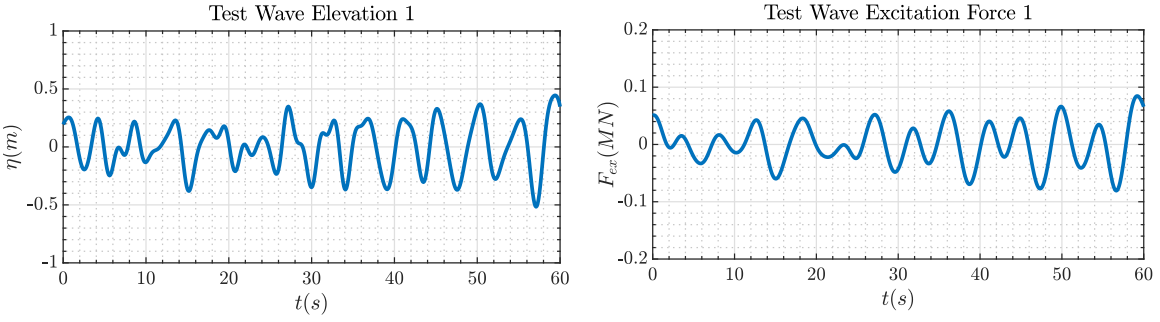

(a) Point 1

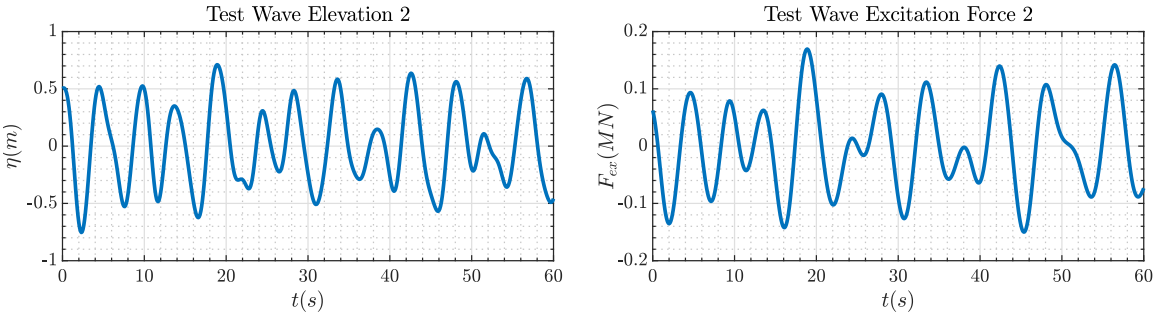

(b) Point 2

Fig. 12. 60 s ahead forecasted wave elevations and relevant wave excitation forces exerted on the considered point absorber WEC of the selected locations to evaluate the performance of the controller.

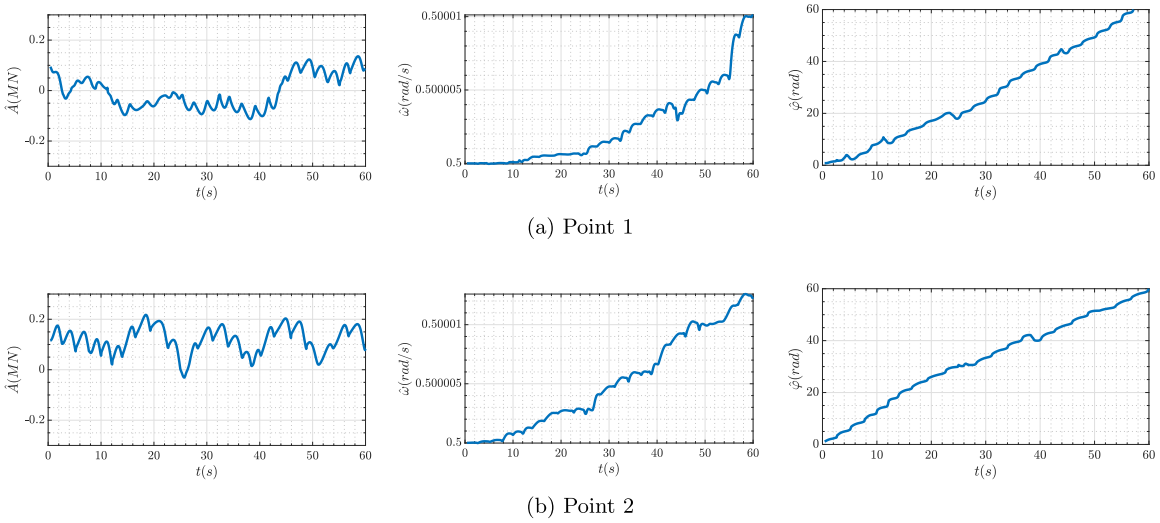

(a) Point 1

(b) Point 2

Fig. 13. Real-time estimations of the amplitude $\hat{A}(t)$, frequency $\hat{\omega}(t)$, and phase $\hat{\varphi}(t)$ of the selected locations' test wave excitation forces by the MHE-EKF method.

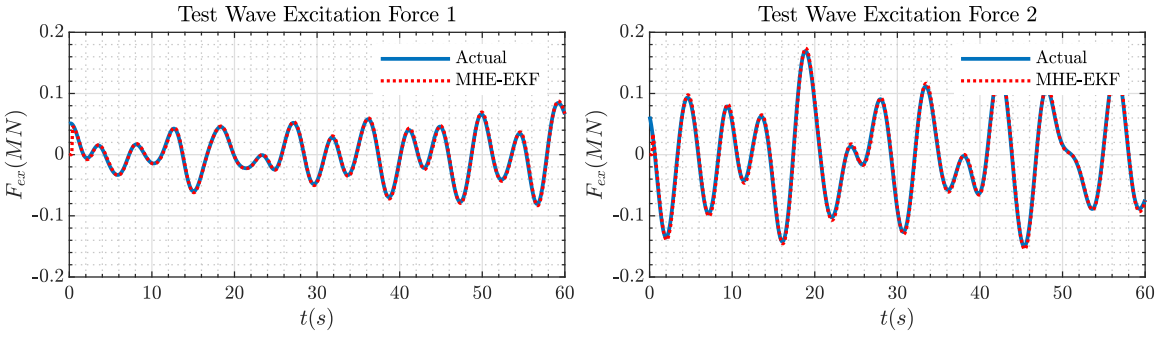

Fig. 14. Time series of the test wave excitation force actual values exerted on the considered point absorber WEC vs. MHE-EKF method outputs of the selected points.

to produce updated estimates $\hat{A}(t)$, $\hat{\omega}(t)$, and $\hat{\varphi}(t)$, which are then substituted into (44) to reconstruct the excitation force signal $\hat{F}_{\text{ex}}(t)$. Moreover, Fig. 14 depicts the time-series data of both the test actual wave excitation forces exerted on the analyzed WEC and their estimates obtained through the MHE-EKF method. As evidenced by this figure, the estimated values by MHE-EKF method closely align with the actual values, indicating a satisfactory level of accuracy in the estimation process. Finally, the time series of the generated non-constrained WEC reference velocities of the selected points are illustrated in Fig. 15. The WEC controller should be designed in such a way that it can track these signals as much as possible.

7.4. Control strategy performance evaluation

7.4.1. Performance evaluation on the selected sea states

In this subsection, the effectiveness of the proposed control strategy is evaluated on the sea states of the selected studied points. Time-domain simulations are performed utilizing MATLAB software. The variable-step explicit Runge–Kutta (4,5) is applied to solve the coupled ordinary differential equations (ODEs). While the explicit Runge–Kutta method was selected for its robustness and ease of implementation, alternative methods, such as implicit solvers and multi-rate time-stepping techniques, could offer advantages in terms of stability and computational efficiency. Implicit solvers are particularly useful for stiff systems, while multi-rate time-stepping techniques can be beneficial for simulating systems with different time scales. The simulations aim to follow the reference velocities generated by Eq. (48) while minimizing deviations in the presence of disturbances $F_{ex}(t)$. Moreover, it is assumed there are no constraints on the PTO force and the WEC body displacements.

According to the results of the analysis in the frequency domain, the state space matrices of the considered WEC are as follows

$$A = \begin{bmatrix} 0 & 1 & 0 & 0 & 0 \\ -1.907105 & 0 & 0.064919 & -0.003229 & -0.030018 \\ 0 & -2.511690 & -0.913479 & 1.173820 & 0.954371 \\ 0 & -0.124915 & -1.173820 & -0.002449 & -0.040506 \\ 0 & -1.161395 & -0.954371 & -0.040506 & -1.710239 \end{bmatrix}$$

$$B = \begin{bmatrix} 0 \\ 3.782422 \times 10^{-6} \\ 0 \\ 0 \\ 0 \end{bmatrix}, \quad C = \begin{bmatrix} 1 & 0 & 0 & 0 & 0 \\ 0 & 1 & 0 & 0 & 0 \end{bmatrix}, \quad D = \begin{bmatrix} 0 \\ 0 \end{bmatrix}$$

Other matrices are determined as

$$Q = 10^{10} \times \begin{bmatrix} 9 & 9 \\ 9 & 9 \end{bmatrix}, \quad Z = \begin{bmatrix} 0 \\ -1 \\ 0 \\ 0 \\ 0 \end{bmatrix}, \quad R = 0.00001$$

It is necessary to explain that the matrix elements of Q and R are selected by trial and error. The values of these matrices depend on the considered problem.

Fig. 16 shows the tracking results of the reference displacement and velocity by the proposed control strategy for studied irregular waves of the selected points. According to this figure, generally, it

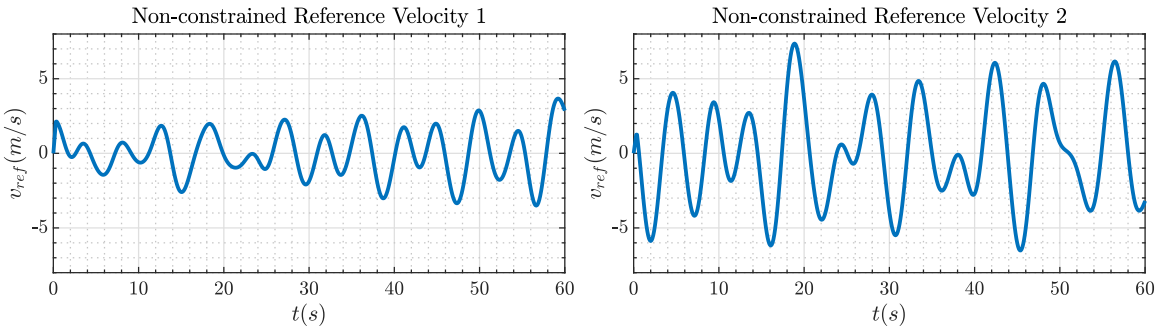

Fig. 15. Time series of the non-constrained reference velocities of the selected points.

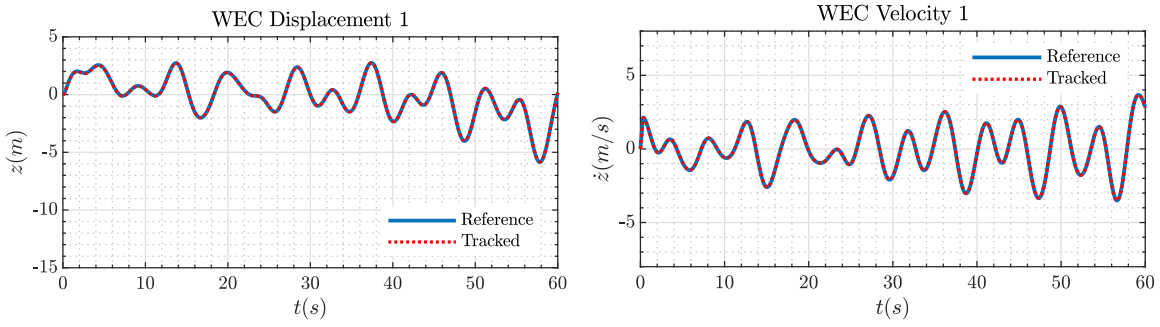

(a) Point 1

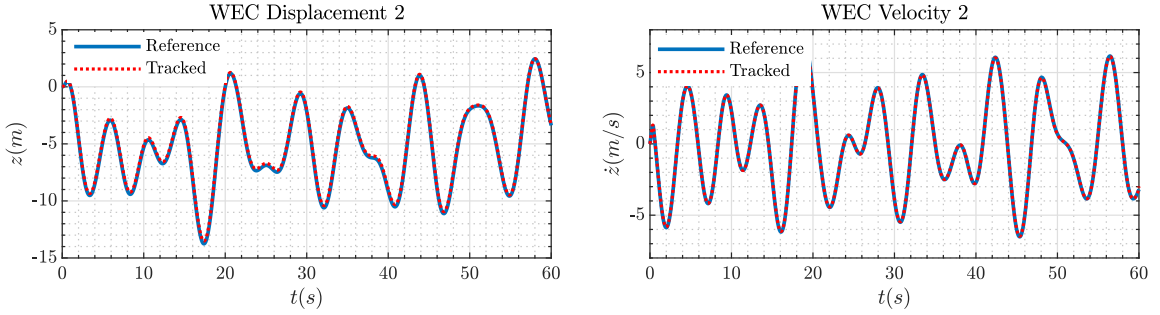

(b) Point 2

Fig. 16. Tracking results of the reference displacement and velocity by the proposed control strategy for studied irregular waves of the selected points.

can be said that the close matching observed between the reference and the tracked signals underscores the robustness and effectiveness of the proposed controller. The time series of the calculated PTO force of these two considered sea states is depicted in Fig. 17. Moreover, the time series of the absorbed power, $P_{\text{abs}}(t) = F_{\text{PTO}}(t) \cdot \dot{z}(t)$, in both cases are illustrated in Fig. 18. In this figure, it should be noted that negative power typically indicates that energy is being extracted from the system rather than being supplied to it. When a WEC is generating power, it produces positive power, indicating that it is converting the kinetic energy of the waves into electrical energy or some other form of usable energy. However, during certain conditions or phases of operation, a WEC may consume more energy than it generates. This can happen, for example, when the waves are too small for the WEC to effectively capture and convert their energy, or during startup phases when the device consumes power but is not yet producing significant energy output. In such cases, the power generated by the WEC may be negative, indicating that the device is consuming power from an external source or dissipating energy rather than generating it. This is not desirable from an efficiency standpoint but can be part of the operational characteristics of certain WEC designs. Moreover, in the investigated case, no constraints are defined for the WEC velocity and PTO force. Hence, the value of the negative power may be large in some time steps.

As mentioned, the values of weight matrices Q and R can have considerable effects on the WEC controller's performance. Two different cases are considered to investigate the effects of Q and R variations on the performance of the studied WEC controller by calculating the Root Mean Square Error (RMSE) of the reference velocity tracking of both considered sea states. In the first case, only the value of the scalar R is changed from 0.00001 to 1 with 20 linearly spaced time steps. The rest of the parameters and conditions are considered constant. In the second case, all the parameters and conditions are considered constant, only the elements of the Q matrix are changed. $Q = \alpha \cdot \begin{bmatrix} 1 & 1 \\ 1 & 1 \end{bmatrix}$ is assumed, where α value is changed from 3.0e7 to 9.0e10. The results are shown in Fig. 19. As it is clear in this figure, by reducing the value of R, the error value is also reduced. Moreover, the error value is decreased by

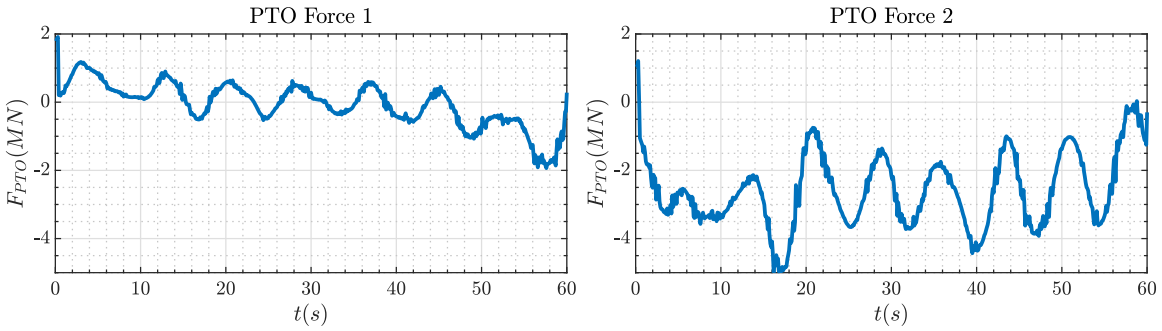

Fig. 17. Time series of the PTO force calculated by the proposed control strategy for studied irregular waves of the selected points.

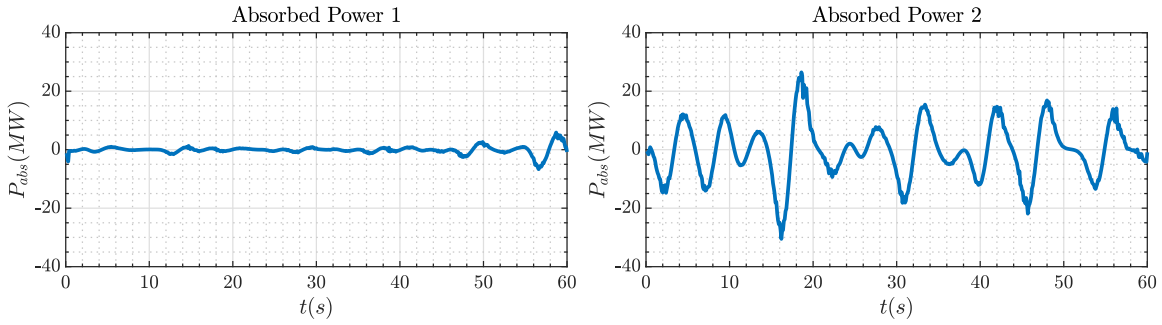

Fig. 18. Time series of the absorbed power in the presence of the controller for studied irregular waves of the selected points.

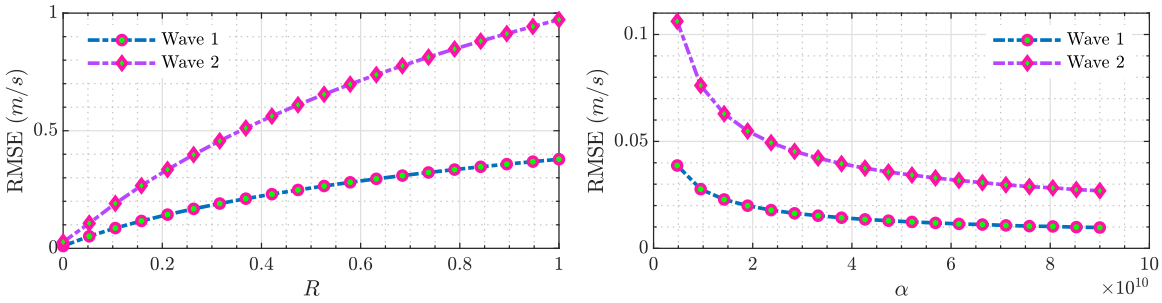

Fig. 19. The effects of weight matrices Q and R on the velocity tracking performance of the considered WEC for studied irregular waves of the selected points. $Q = \alpha \cdot \begin{bmatrix} 1 & 1 \\ 1 & 1 \end{bmatrix}$.

increasing the element values of the Q matrix. It should be noted that this occurred in the investigated case; however, in general, the values of the matrices Q and R should be chosen relative to each other.

7.4.2. Performance evaluation concerning the WEC dynamics variations

Several factors can influence the dynamics of the WEC system. As mentioned, the proposed control strategy can handle the dynamic variations of the WEC system. It adapts seamlessly to changes in environmental conditions, ensuring optimal energy capture efficiency across diverse operational scenarios. To investigate this capability, the dynamics of the WEC system suddenly changed during the control operation and it is checked whether it can follow the WEC reference velocity or not. For this purpose, the performance of the controller is investigated within 120 s of execution and after the 60th second, the dynamics of the system is changed. The WEC under consideration here is the one described in Section 2.1. The only parameter that is changed after 60 s of the control execution is the WEC draught. Therefore, the value of the draught parameter is 5 m from 0 to 60 s, and after that and up to 120 s, it is 6 m. It is necessary to explain that the change of this parameter changes other dynamics parameters of the system such as mass and added mass. The mass properties of the WEC, when draught is 5 m, are shown in Table 1, and the mass properties of the new case are presented in Table 6. Other hydrodynamic frequency domain parameters are shown in Table 3. The wave considered here is generated using the JONSWAP spectrum with $H_s = 2$ m, $T_p = 8$ s, and $\gamma = 2$. In this case, it is assumed that the wave excitation forces information of both WEC dynamics are already available to use in the controller. The results of displacement and velocity tracking are provided in Fig. 20. As evident in this figure, in this scenario as well, the presented control theory has been able to track the reference signals with acceptable accuracy in the presence of disturbance and maintain its functionality despite the change in system dynamics. This shows the power of the proposed control strategy against the dynamic changes in the system. Although this study evaluates single-parameter changes, the adaptive control framework is designed to accommodate multi-parameter variations by utilizing real-time feedback to adjust control actions dynamically. This real-time adaptability ensures that the control strategy can respond promptly to changes in the WEC's operating environment which maintains optimal performance and stability. It is necessary to emphasize again that in this research, the WEC reference velocity is calculated without any constraints. In the practical sense,

Table 6
The mass properties of the considered point absorber WEC when draught is 6 m.

Parameter	Value	Unit
Center of gravity (CoG) position concerning the global axis	$x = 0, y = 0, z = -3.4985$	m
Body mass	240436.5578	kg
Volumetric displacement	234.5723	m^3
Moment of inertia around the x-axis (I_{xx})	2078613.9313	$kg.m^2$
Moment of inertia around the y-axis (I_{yy})	2078613.9313	$kg.m^2$
Moment of inertia around the z-axis (I_{zz})	1538954.8192	$kg.m^2$

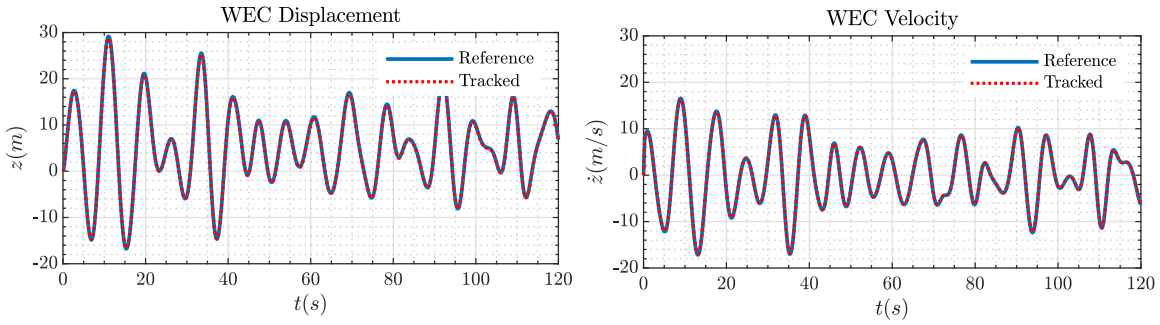

Fig. 20. Tracking results of the reference displacement and velocity by the proposed control strategy when the dynamic of the system changes for a wave generated using the JONSWAP spectrum with $H_s = 2$ m, $T_p = 8$ s, and $\gamma = 2$.

reaching these limits of displacement and velocity, which is shown in Fig. 20, is very difficult and requires a huge source of PTO force. Moreover, while the current analysis assumes aligned initial conditions for simplicity, a significant mismatch could impact performance during the transient phase. This can be mitigated by employing initialization strategies such as pre-tuning controller parameters, adaptive initialization phases, or incorporating state observers to estimate and align initial conditions dynamically.

It is necessary to explain that in the previously presented results, it is assumed that the initial conditions of the reference signals and the start of the controller are the same. But in general, the initial conditions may not be the same, where in this case the controller needs some time to adapt to the conditions and track the reference signals. Fig. 21 illustrates this case where the controller has been able to track the reference signals after a while. Moreover, in the presented results, it is assumed that the time of applying the controller corresponds to the start time of the reference signals. But in general, the controller may apply after some delays. In this case, the controller should be able to track the reference signals with acceptable accuracy. Fig. 22 shows this case. As it is clear in this figure, the controller is applied after 20 s and can track the reference signals with high accuracy.

7.4.3. Discussion

The presented results demonstrate the effectiveness of the proposed control strategy in adapting to varying wave climates and WEC dynamics. However, a direct quantitative comparison with existing literature is not feasible due to inherent differences in case study configurations, including WEC designs, wave climates, PTO setup, and control strategies. Such variations significantly influence performance metrics. Instead, the findings are contextualized by identifying their alignment with broader trends observed in wave energy research. For instance, the demonstrated improvements in power absorption and the controller's ability to adapt to sudden changes in system dynamics are consistent with the findings of recent studies that emphasize the importance of adaptive control techniques [30,31,60]. Additionally, the integration of wave elevation forecasting using neural networks with the controller is an innovative approach that extends the existing body of research by addressing practical constraints such as limited real-time data availability and computational efficiency. Furthermore, this research emphasis on realistic sea states and dynamic system variations addresses key limitations of many existing studies that rely on idealized assumptions.

A comprehensive frequency and time domain modeling framework for the considered WEC has been developed and described. This includes detailed setup parameters and modeling assumptions, enabling other researchers to reproduce and build upon this work. This research emphasizes transparency in modeling which makes it a robust reference point for future investigations. This study evaluates the performance of the proposed control strategy using realistic sea states, ensuring practical applicability. Instead of relying on simplified or idealized wave conditions, which are common in many studies, irregular waves and site-specific sea states are considered to mimic real-world scenarios. Moreover, a unique feature of this study is the generation of reference velocities that the controller uses for tracking. These velocities are derived to ensure that the WEC's body oscillation velocity remains in phase with the wave excitation force, maximizing power production. While other studies often overlook this critical aspect, this research highlights its importance in optimizing energy extraction.

A key strength of this work is the thorough evaluation of the proposed control strategy across different scenarios: The controller's ability to accurately track reference WEC displacements and velocities was rigorously tested. The results demonstrate its robustness and adaptability, even under fluctuating wave conditions. The study evaluates the controller's performance when the WEC dynamics vary, such as changes in system mass or hydrodynamic coefficients. This adaptability is a key factor for real-world applications where system parameters can change over time. To simulate realistic scenarios where the controller might be activated after some delay, tracking performance is assessed when the controller turned on after several seconds. This analysis is rare in existing literature and provides valuable insights into real-world operational challenges.

8. Conclusion

This research presented an innovative framework aimed at mitigating disturbances affecting WECs through adaptive optimal disturbance rejection. By dynamically adjusting control actions based on forecasted wave conditions, this approach sought to enhance the efficiency and reliability of WECs across diverse operating environments. Through accurate analysis, the paper demonstrated the adaptability and effectiveness of the proposed approach in tracking displacement and

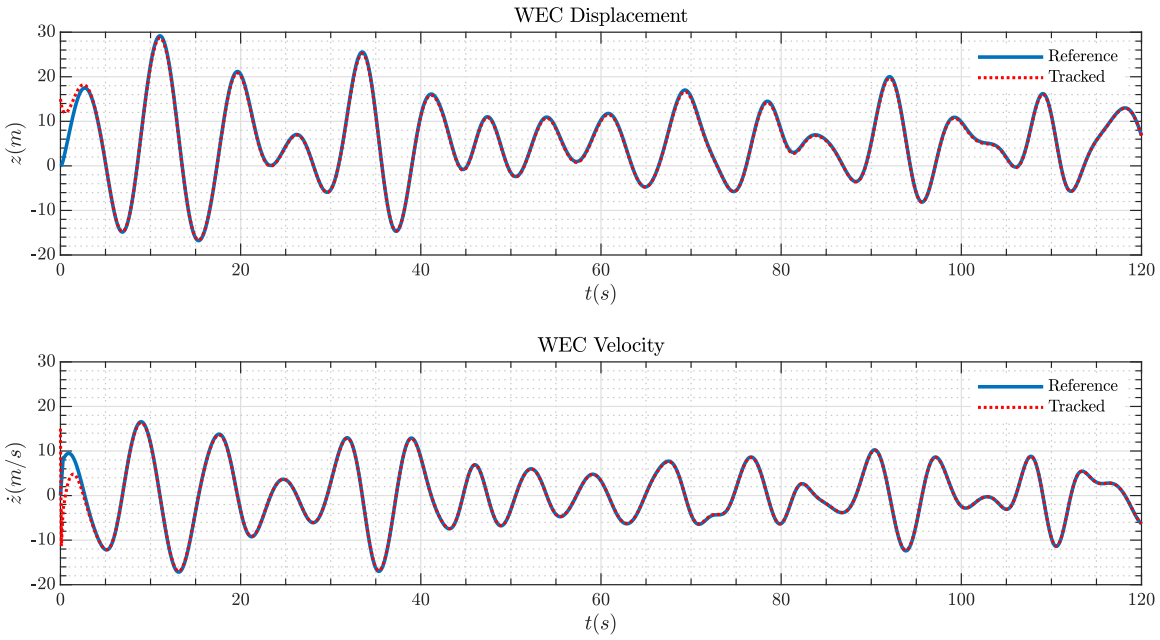

Fig. 21. Tracking results of the reference displacement and velocity by the proposed control strategy when the dynamic of the system changes for a wave generated using the JONSWAP spectrum with $H_s = 2$ m, $T_p = 8$ s, and $\gamma = 2$ with initial conditions far from the reference signals starting points.

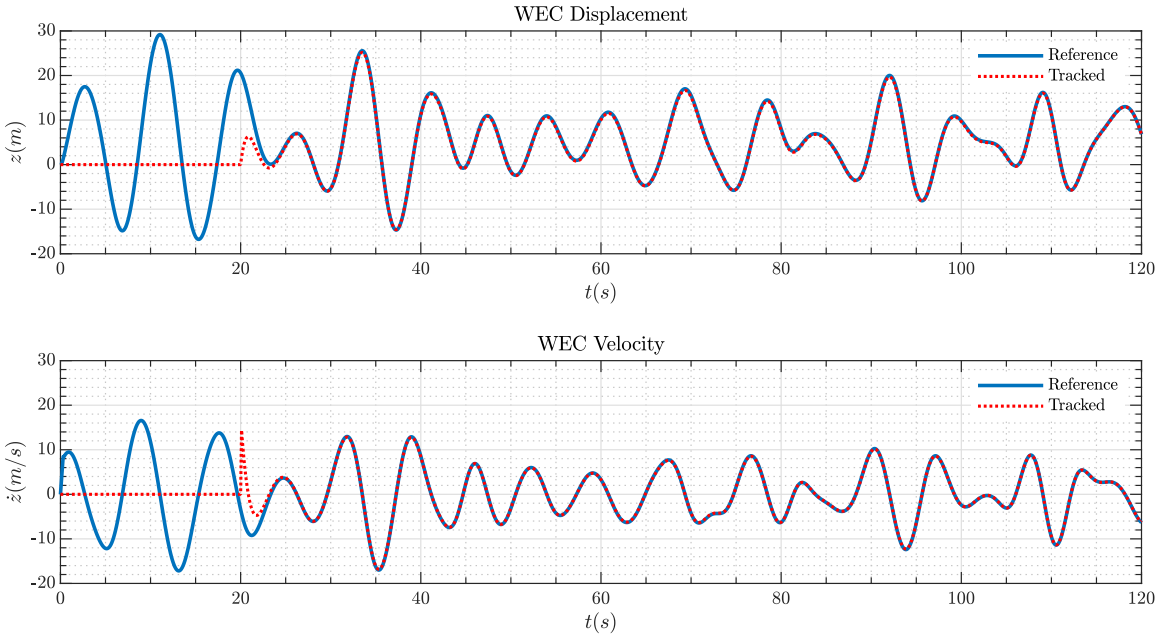

Fig. 22. Tracking results of the reference displacement and velocity by the proposed control strategy when the dynamic of the system changes for a wave generated using the JONSWAP spectrum with $H_s = 2$ m, $T_p = 8$ s, and $\gamma = 2$. The controller is applied after 20 s.

velocity reference signals with high precision, even in the presence of external disturbances. Through this research, the goal is to contribute to the advancement of control strategies for WECs which offer a pathway toward more efficient and reliable exploitation of wave energy resources. While this study focuses on a single-body heaving point absorber, the proposed control strategy could be extended to multi-body or articulated WEC systems. The adaptive control framework presented here can be adapted to handle the complexities of multi-body systems by incorporating coupled models to account for the dynamic interactions between individual bodies. This study has some limitations that are necessary to consider. The controller's performance was evaluated under specific wave conditions and may require additional validation for highly irregular or extreme wave environments. Hydrodynamic coefficients were obtained through linear potential flow theory, which may not capture highly nonlinear interactions in extreme sea states. Finally, the study focuses on a single-body WEC in heave motion, limiting the applicability of findings to other WEC designs or multi-degree-of-freedom systems. Future research could investigate deeper into the robustness of the control strategy under multi-degree-of-freedom dynamics with complex WEC geometries and validate its efficacy through practical implementations. Moreover, future research could explore a comparative analysis between traditional forecasting methods and advanced machine learning techniques. This

investigation should specifically focus on evaluating their respective strengths and weaknesses, particularly in terms of prediction accuracy and computational demand. Furthermore, to further enhance the practical applicability of the proposed control strategy, future research should explore the integration of constraint-handling techniques for PTO force and motion limits.

CRediT authorship contribution statement

Kumars Mahmoodi: Writing – review & editing, Writing – original draft, Visualization, Validation, Software, Resources, Methodology, Investigation, Formal analysis, Data curation, Conceptualization. **Abolhassan Razminia:** Writing – review & editing, Writing – original draft, Methodology, Investigation, Conceptualization. **Jari Böling:** Writing – review & editing, Writing – original draft, Software, Methodology, Investigation, Funding acquisition.

Ethical approval

This paper is the authors' original work and has not been previously published elsewhere.

Declaration of Generative AI and AI-assisted technologies in the writing process

During the preparation of this work, the authors used ChatGPT and Microsoft Copilot to refine the language and improve clarity. After using this tool, the authors reviewed and edited the content as needed and take full responsibility for the content of the publication.

Funding

This research is supported by the Business Finland project INDECS with grant number 7682/31/2022, Finland.

Declaration of competing interest

The authors declared no potential conflicts of interest with respect to the research, authorship, and/or publication of this article.

Acknowledgments

The authors extend their gratitude to the reviewers for their detailed evaluation and constructive feedback, which have undoubtedly strengthened the quality of the paper.

Data availability

Data will be made available on request.

References

[1] Mahmoodi K, Saybani M, Azad ST. A temporal and spatial resolution wind and wave power resource assessment in the Oman Gulf. Ocean Eng 2022;249:110881. http://dx.doi.org/10.1016/j.oceaneng.2022.110881.

[2] Martinez-Iturricastillo N, Nic Guidhir M, Ulazia A, Ringwood JV. Extreme wave analysis for marine renewable energies in Ireland. Energy Convers Manag: X 2025;26:100972. http://dx.doi.org/10.1016/j.ecmx.2025.100972, URL https://www.sciencedirect.com/science/article/pii/S2590174525001047.

[3] Durand S, Turcotte P, Haillot D, Rousse DR, Arasteh H, Kalivogui S, et al. Decarbonization strategies for northern Canada: A review of renewable energy and energy storage in off-grid communities. Energy Convers Manag: X 2025;27:101055. http://dx.doi.org/10.1016/j.ecmx.2025.101055, URL https://www.sciencedirect.com/science/article/pii/S2590174525001874.

[4] Mosquera FD, Evangelista CA, Puleston PF, Ringwood JV. Adaptive second order sliding mode control of an oscillating water column. IET Renew Power Gener 2024;18(2):226–37. http://dx.doi.org/10.1049/rpg2.12912.

[5] Mahmoodi K, Fard HR, Böling J. Long-term climate change effects on power performance of wave energy converters: A case study. Energy 2025;326:136101. http://dx.doi.org/10.1016/j.energy.2025.136101, URL https://www.sciencedirect.com/science/article/pii/S0360544225017438.

[6] Zhan S, Chen W-H, Steffen T, Ringwood JV. Computationally efficient infinite-horizon indefinite model predictive control with disturbance preview information. Automatica 2022;146:110667. http://dx.doi.org/10.1016/j.automatica.2022.110667.

[7] Ermakov A, Ali ZA, Mahmoodi K, Mason O, Ringwood JV. A frequency domain-based control methodology for performance assessment and optimisation of heterogeneous arrays of wave energy converters. In: 2024 IEEE conference on control technology and applications. 2024, p. 584–9. http://dx.doi.org/10.1109/CCTA60707.2024.10666578.

[8] Rusu L. An evaluation of the synergy between the wave and wind energy along the west Iberian nearshore. Energy Convers Manag: X 2023;20:100453. http://dx.doi.org/10.1016/j.ecmx.2023.100453, URL https://www.sciencedirect.com/science/article/pii/S2590174523001095.

[9] Hasan A, Kayes I, Alam M, Shahriar T, Ahsan Habib M. Generalized machine learning models to predict significant wave height utilizing wind and atmospheric parameters. Energy Convers Manag: X 2024;23:100623. http://dx.doi.org/10.1016/j.ecmx.2024.100623, URL https://www.sciencedirect.com/science/article/pii/S2590174524001016.

[10] Arredondo-Galeana A, Ermakov A, Shi W, Ringwood JV, Brennan F. Control strategies for power enhancement and fatigue damage mitigation of wave cycloidal rotors. 2022, http://dx.doi.org/10.2139/ssrn.4346306, Available At SSRN 4346306.

[11] Penalba M, Giorgi G, Ringwood JV. Mathematical modelling of wave energy converters: A review of nonlinear approaches. Renew Sustain Energy Rev 2017;78:1188–207. http://dx.doi.org/10.1016/j.rser.2016.11.137.

[12] Mahmoodi K, Razminia A, Ghassemi H. Optimal control of wave energy converters with non-integer order performance indices: A dynamic programming approach. Renew Energy 2021;177:1212–33. http://dx.doi.org/10.1016/j.renene.2021.06.045.

[13] Carrelhas A, Gato L. Reliable control of turbine–generator set for oscillating-water-column wave energy converters: Numerical modelling and field data comparison. Energy Convers Manage 2023;282:116811. http://dx.doi.org/10.1016/j.enconman.2023.116811, URL https://www.sciencedirect.com/science/article/pii/S0196890423001577.

[14] Said HA, García-Violini D, Ringwood JV. Wave-to-grid (W2G) control of a wave energy converter. Energy Convers Manag: X 2022;14:100190. http://dx.doi.org/10.1016/j.ecmx.2022.100190, URL https://www.sciencedirect.com/science/article/pii/S2590174522000137.

[15] Ermakov AM, Ali ZA, Mahmoodi K, Mason O, Ringwood JV. Optimisation of heterogeneous wave energy converter arrays: A control co-design strategy. Renew Energy 2025;244:122637. http://dx.doi.org/10.1016/j.renene.2025.122637, URL https://www.sciencedirect.com/science/article/pii/S096014812500299X.

[16] Zhang M, Yu S-R, Zhao G-W, Dai S-S, He F, Yuan Z-M. Model predictive control of wave energy converters. Ocean Eng 2024;301:117430. http://dx.doi.org/10.1016/j.oceaneng.2024.117430.

[17] Wang L, Isberg J, Tedeschi E. Review of control strategies for wave energy conversion systems and their validation: the wave-to-wire approach. Renew Sustain Energy Rev 2018;81:366–79. http://dx.doi.org/10.1016/j.rser.2017.06.074.

[18] Fard HR, Mahmoodi K, Vaghefi M. Geometry optimization of a two-body heaving point absorber wave energy converter based on the long-term Oman Gulf wave climate. Renew Energy 2025;253:123498. http://dx.doi.org/10.1016/j.renene.2025.123498, URL https://www.sciencedirect.com/science/article/pii/S0960148125011607.

[19] Yang B, Duan J, Chen Y, Wu S, Li M, Cao P, et al. A critical survey of power take-off systems based wave energy converters: Summaries, advances, and perspectives. Ocean Eng 2024;298:117149. http://dx.doi.org/10.1016/j.oceaneng.2024.117149.

[20] Shadmani A, Nikoo MR, Gandomi AH, Wang R-Q, Golparvar B. A review of machine learning and deep learning applications in wave energy forecasting and WEC optimization. Energy Strat Rev 2023;49:101180. http://dx.doi.org/10.1016/j.esr.2023.101180.

[21] Zou S, Zhou X, Weaver W, Abdelkhalik O. Deep reinforcement learning control of wave energy converters. IFAC-PapersOnLine 2022;55(27):305–10. http://dx.doi.org/10.1016/j.ifacol.2022.10.530, URL https://www.sciencedirect.com/science/article/pii/S2405896322025836. 9th IFAC Symposium on Mechatronic Systems MECHATRONICS 2022.

[22] Su H, Qin H, Wen Z, Liang H, Jiang H, Mu L. Optimization of latching control for duck wave energy converter based on deep reinforcement learning. Ocean Eng 2024;309:118531. http://dx.doi.org/10.1016/j.oceaneng.2024.118531, URL https://www.sciencedirect.com/science/article/pii/S0029801824018699.

[23] Wang H, Wijaya V, Zeng T, Zhang Y. Deep reinforcement learning-based non-causal control for wave energy conversion. Ocean Eng 2024;311:118860. http://dx.doi.org/10.1016/j.oceaneng.2024.118860, URL https://www.sciencedirect.com/science/article/pii/S002980182402198X.

[24] Yin X, Jiang Z. Wave condition preview assisted real-time nonlinear predictive control of point-absorbing wave energy converter based on long short-term memory recurrent neural identification. Mech Syst Signal Process 2023;188:109669. http://dx.doi.org/10.1016/j.ymssp.2022.109669, URL https://www.sciencedirect.com/science/article/pii/S0888327022007506.
[25] Zhang M, Yu S-R, Zhao G-W, Dai S-S, He F, Yuan Z-M. Model predictive control of wave energy converters. Ocean Eng 2024;301:117430. http://dx.doi.org/10.1016/j.oceaneng.2024.117430, URL https://www.sciencedirect.com/science/article/pii/S0029801824007674.
[26] Zhang M, Yuan Z-M, Dai S-S, Chen M-L, Incecik A. LSTM RNN-based excitation force prediction for the real-time control of wave energy converters. Ocean Eng 2024;306:118023. http://dx.doi.org/10.1016/j.oceaneng.2024.118023, URL https://www.sciencedirect.com/science/article/pii/S0029801824013611.
[27] Lei Y. A wave forecasting method based on probabilistic diffusion LSTM network for model predictive control of wave energy converters. Appl Soft Comput 2024;164:112006. http://dx.doi.org/10.1016/j.asoc.2024.112006, URL https://www.sciencedirect.com/science/article/pii/S1568494624007804.
[28] Arrosyid WA, Sari WR, Waskito KT, Yanuar, Pria Utama IKA, Binu Soesanto QM, et al. Recent advancements in wave energy converter technologies: A comprehensive review on design and performance optimization. Ocean Eng 2025;340:122328. http://dx.doi.org/10.1016/j.oceaneng.2025.122328, URL https://www.sciencedirect.com/science/article/pii/S0029801825020128.
[29] Pasta E, Faedo N, Mattiazzo G, Ringwood JV. Towards data-driven and data-based control of wave energy systems: Classification, overview, and critical assessment. Renew Sustain Energy Rev 2023;188:113877. http://dx.doi.org/10.1016/j.rser.2023.113877, URL https://www.sciencedirect.com/science/article/pii/S1364032123007359.
[30] Zhan S, Wang B, Na J, Li G. Adaptive optimal control of wave energy converters. IFAC-PapersOnLine 2018;51(29):38–43. http://dx.doi.org/10.1016/j.ifacol.2018.09.466, 11th IFAC Conference on Control Applications in Marine Systems, Robotics, and Vehicles CAMS 2018.
[31] Davidson J, Genest R, Ringwood JV. Adaptive control of a wave energy converter. IEEE Trans Sustain Energy 2018;9(4):1588–95. http://dx.doi.org/10.1109/TSTE.2018.2798921.
[32] Zhang Y, Bian J, Huang Z. Built-in wave energy converter inspired adaptive vibration control for offshore floating platform. Renew Energy 2025;254:123679. http://dx.doi.org/10.1016/j.renene.2025.123679, URL https://www.sciencedirect.com/science/article/pii/S0960148125013412.
[33] Mahmoodi K, Nepomuceno E, Razminia A. Wave excitation force forecasting using neural networks. Energy 2022;247:123322. http://dx.doi.org/10.1016/j.energy.2022.123322.
[34] Zhan S, Na J, Li G, Wang B. Adaptive model predictive control of wave energy converters. IEEE Trans Sustain Energy 2020;11(1):229–38. http://dx.doi.org/10.1109/TSTE.2018.2889767.
[35] Nguyen H-N. Adaptive PI control of wave energy converters with force and motion constraints. IEEE Trans Sustain Energy 2024;15(2):747–57. http://dx.doi.org/10.1109/TSTE.2023.3301732.
[36] Wang N, Deng Z. Finite-time fault estimator based fault-tolerance control for a surface vehicle with input saturations. IEEE Trans Ind Inform 2020;16(2):1172–81. http://dx.doi.org/10.1109/TII.2019.2930471.
[37] Wang N, Su S-F. Finite-time unknown observer-based interactive trajectory tracking control of asymmetric underactuated surface vehicles. IEEE Trans Control Syst Technol 2021;29(2):794–803. http://dx.doi.org/10.1109/TCST.2019.2955657.
[38] Do DK. Nonlinear control with wave observer to maximize harvested power for point absorber wave energy converters. Asian J Control 2022;24(1):16–45. http://dx.doi.org/10.1002/asjc.2461.
[39] Zhang C, Wang N. Finite-time observer-based path-following control of an underactuated surface vehicle with actuator saturation and fault. In: 2024 international conference on fuzzy theory and its applications. 2024, p. 1–6. http://dx.doi.org/10.1109/iFUZZY63051.2024.10662885.
[40] Papini G, Faedo N, Mattiazzo G, et al. Observer-based fault estimation applied to a point absorber wave energy converter. In: Proceedings of the European wave and tidal energy conference, vol. 15, 2023, http://dx.doi.org/10.36688/ewtec-2023-375.
[41] Simorgh A, Razminia A, Machado JT. Optimal control of nonlinear fed-batch process using direct transcription method. Comput Chem Eng 2019;130:106561. http://dx.doi.org/10.1016/j.compchemeng.2019.106561.
[42] Mahmoodi K, Ghassemi H, Razminia A. Performance assessment of a two-body wave energy converter based on the Persian Gulf wave climate. Renew Energy 2020;159:519–37. http://dx.doi.org/10.1016/j.renene.2020.06.071.
[43] Zhang Z, Qin J, Wang D, Wang W, Liu Y, Xue G. Research on wave excitation estimators for arrays of wave energy converters. Energy 2023;264:126133. http://dx.doi.org/10.1016/j.energy.2022.126133.
[44] Ruehl K, Michelen C, Kanner S, Lawson M, Yu Y-H. Preliminary verification and validation of WEC-sim, an open-source wave energy converter design tool. In: International conference on offshore mechanics and arctic engineering, vol. 45547, American Society of Mechanical Engineers; 2014, http://dx.doi.org/10.1115/omae2014-24312, V09BT09A040.
[45] Kung S-Y. A new identification and model reduction algorithm via singular value decomposition. In: Proc. 12th asilomar conf. on circuits, systems and computer. 1978, p. 705–14, URL https://api.semanticscholar.org/CorpusID:115891362.
[46] Taghipour R, Perez T, Moan T. Hybrid frequency–time domain models for dynamic response analysis of marine structures. Ocean Eng 2008;35(7):685–705. http://dx.doi.org/10.1016/j.oceaneng.2007.11.002.
[47] Ringwood JV, Zhan S, Faedo N. Empowering wave energy with control technology: Possibilities and pitfalls. Annu Rev Control 2023;55:18–44. http://dx.doi.org/10.1016/j.arcontrol.2023.04.004, URL https://www.sciencedirect.com/science/article/pii/S1367578823000226.
[48] Zhang Z, Wang J, Wei D, Luo T, Xia Y. A novel ensemble system for short-term wind speed forecasting based on two-stage attention-based recurrent neural network. Renew Energy 2023;204:11–23. http://dx.doi.org/10.1016/j.renene.2022.12.120, URL https://www.sciencedirect.com/science/article/pii/S0960148122019188.
[49] Lu P, Yang J, Ye L, Zhang N, Wang Y, Di J, et al. A novel adaptively combined model based on induced ordered weighted averaging for wind power forecasting. Renew Energy 2024;226:120350. http://dx.doi.org/10.1016/j.renene.2024.120350, URL https://www.sciencedirect.com/science/article/pii/S0960148124004154.
[50] Balkissoon S, Fox N, Lupo A, Haupt SE, Penny SG. Classification of tall tower meteorological variables and forecasting wind speeds in Columbia, Missouri. Renew Energy 2023;217:119123. http://dx.doi.org/10.1016/j.renene.2023.119123, URL https://www.sciencedirect.com/science/article/pii/S0960148123010376.
[51] Abbasian Hamedani E, Talebi S. Modeling and long-term forecasting of CO2 emissions in Asia: An optimized Artificial Neural Network approach with consideration of renewable energy scenarios. Energy Convers Manag: X 2025;26:101030. http://dx.doi.org/10.1016/j.ecmx.2025.101030, URL https://www.sciencedirect.com/science/article/pii/S259017452500162X.
[52] Mahmoodi K, Ghassemi H, Razminia A. Wind energy potential assessment in the Persian Gulf: a spatial and temporal analysis. Ocean Eng 2020;216:107674. http://dx.doi.org/10.1016/j.oceaneng.2020.107674.
[53] Mahmoodi K, Ghassemi H, Razminia A. Temporal and spatial characteristics of wave energy in the Persian Gulf based on the ERA5 reanalysis dataset. Energy 2019;187:115991. http://dx.doi.org/10.1016/j.energy.2019.115991.
[54] Hasan M, Mifta Z, Papiya SJ, Roy P, Dey P, Salsabil NA, et al. A state-of-the-art comparative review of load forecasting methods: Characteristics, perspectives, and applications. Energy Convers Manag: X 2025;26:100922. http://dx.doi.org/10.1016/j.ecmx.2025.100922, URL https://www.sciencedirect.com/science/article/pii/S2590174525000546.
[55] Fusco F, Ringwood JV. A simple and effective real-time controller for wave energy converters. IEEE Trans Sustain Energy 2012;4(1):21–30. http://dx.doi.org/10.1109/TSTE.2012.2196717.
[56] Fusco F, Ringwood JV. Hierarchical robust control of oscillating wave energy converters with uncertain dynamics. IEEE Trans Sustain Energy 2014;5(3):958–66. http://dx.doi.org/10.1109/TSTE.2014.2313479.
[57] Quine B, Uhlmann J, Durrant-Whyte H. Implicit Jacobian for linearised state estimation in nonlinear systems. In: Proceedings of 1995 American control conference, vol. 3, IEEE; 1995, p. 1645–6. http://dx.doi.org/10.1109/ACC.1995.529787.
[58] Fusco F, Ringwood JV. Short-term wave forecasting for real-time control of wave energy converters. IEEE Trans Sustain Energy 2010;1(2):99–106. http://dx.doi.org/10.1109/TSTE.2010.2047414.
[59] Finnish Meteorological Institute. Finnish Meteorological Institute. 2024, https://en.ilmatieteenlaitos.fi/. (Accessed 1 April 2024).
[60] Nguyen H-N, Tona P. An efficiency-aware continuous adaptive proportional-integral velocity-feedback control for wave energy converters. Renew Energy 2020;146:1596–608. http://dx.doi.org/10.1016/j.renene.2019.07.093, URL https://www.sciencedirect.com/science/article/pii/S0960148119311139.